Supporting Information

For

Access to a Cu^{II}–O–Cu^{II} Motif: Spectroscopic Properties, Solution Structure, and Reactivity

Peter Haack, Anne Kärgel, Claudio Greco, Jadranka Dokic, Beatrice Braun, Florian F. Pfaff, Stefan Mebs, Kallol Ray, and Christian Limberg*

Humboldt-Universität zu Berlin, Institut für Chemie, Brook-Taylor-Str. 2, 12489 Berlin, Germany

E-mail: Christian.limberg@chemie.hu-berlin.de

Experimental Section

General Considerations. All manipulations were carried out in a glove-box, or else by means of Schlenk-type techniques involving the use of a dry argon atmosphere. The ^{1}H, ^{13}C, ^{19}F and ^{31}P NMR spectra were recorded on a Bruker DPX 300 NMR spectrometer (^{1}H 300.1 MHz, ^{13}C 75.5 MHz, ^{19}F 282.4 MHz, ^{31}P 121.5 MHz) with dry and degassed acetonitrile-d$_3$ as solvent at 20°C. The ^{1}H NMR spectra were calibrated against the residual proton (1.94 ppm), the ^{13}C NMR spectra against natural abundance ^{13}C resonances of the deuterated solvents (1.24 ppm), the ^{19}F NMR spectra against CFCl$_3$ and the ^{31}P NMR spectra against H$_3$PO$_4$ as external standards. In order to determine the yield of the PPh$_3$ oxidation ^{31}P NMR spectra were recorded ^{1}H coupled and the D1 time was set to 4 s. DOSY NMR experiments were carried out on a Bruker AV 600 (^{1}H 600.1 MHz) with acetonitrile-d$_3$ as solvent including 1 % vol. TMS as a standard. Microanalyses were performed on a Leco CHNS-932 elemental analyser. Infrared (IR) spectra were recorded using samples prepared as KBr pellets or as solutions with acetonitrile as the solvent with a Shimadzu FTIR-8400S spectrometer. Raman spectra (solvent: acetonitrile, concentration: 30 mM, temperature: variable -80 °C, room temperature, controlled via a Bruker heating control unit) were acquired using a Bruker RAM II FT-Raman Module (1064-nm excitation; Nd:YAG laser) and a Horiba Jobin-Yvon LabRAM HR800 confocal Raman Spectrometer (647.1-nm excitation, Kr ion laser, 514.5-nm excitation, Ar ion laser, 441.6-nm excitation, He-Cd laser). UV/Vis spectra were obtained at variable temperatures on an Agilent 8453 UV-Visible spectrophotometer equipped with a Unisoku USP-203-A cryostat. Unless otherwise stated mass spectra (ESI, APCI and ESI/APCI, respectively) were recorded on an Agilent 6210 Time-of-Flight mass spectrometer using a fragmentor voltage of 250 V. The samples were injected directly into the nebulizer. EPR spectra were recorded at the X-band spectrometer ERS 300 (ZWG/Magnettech Berlin/Adlershof, Germany) equipped with a fused quartz Dewar for measurements (T = 77 K, solvent acetonitrile, microwave frequency 9.246 GHz, power 2 mW, modulation 0.125 mT). XAS measurements were performed on NSLS X3B at Brookhaven National Laboratory in New York, USA. Samples were measured in fluorescence mode while simultaneous a Cu-foil was measured as reference. For detailed setup and procedures see XAS part in the SI.

Theory.

DFT calculations, carried out using the B3LYP exchange-correlation functional[1] and the def2-TZVP basis set for all atoms,[2] were performed in order to optimize the (oxo-bridged) model of the complex cation of the *cis* as well as the *trans* isomer of **5**. Counterions were neglected in the calculations. Optimizations were performed both *in vacuo* using the TURBOMOLE program suite.[3] Analytical vibrational frequencies calculation is also available for *vacuum*-optimized structures in TURBOMOLE, therefore the character of the stationary points obtained was checked to confirm the absence of imaginary frequencies.

As for computation of relative stabilities of different isomeric forms and spin states of the models (Table 2, main text), we used total energies not only from optimizations based on the hybrid B3LYP functional, but also from additional optimizations we carried out with the BP86 functional.[4] This procedure stems from the fact that B3LYP is known to overestimate spin-state splitting (an effect of the Hartree-Fock exchange contribution to the total B3LYP energy),[5] as also noticed in previous mechanistic studies on pMMO active site.[6] On the other hand, BP86 is a pure functional, and as such it lacks the HF exchange contribution. More specifically, energy differences in Table 2 were obtained from *in vacuo* geometry optimizations, followed by single point SCF calculations using an implicit treating of solvent effects based on the COSMO continuum solvent model[7] ($\varepsilon = 36.64$ to simulate the solvent acetonitrile), as implemented in TURBOMOLE.

As far as computation of UV/Vis theoretical spectra is concerned, TDDFT analysis was performed after re-optimization of the models at the CAM-B3LYP/def2-TZVP and CAM-B3LYP/def2-SVP levels. This was done in consideration of the higher accuracy of the coulomb-attenuated CAM-B3LYP density functional in the treatment of charge-transfer states, when compared to standard hybrid and pure functionals.[8] Given the unavailability of CAM-B3LYP within TURBOMOLE, we employed the GAUSSIAN09 suite[9] for all TDDFT calculations, and we used the PCM solvent model both for CAM-B3LYP/def2-TZVP geometry optimizations,[10] and for the subsequent simulation of UV-vis spectra.[11]

Materials. All solvents, except *iso*-propanol, were purified, dried, degassed and stored over molecular sieves prior to use. 4,6-diiododibenzofuran,[12] HN((CH$_2$)$_2$N(CH$_3$)$_2$)(CH$_2$(2-py)),[13] 2-(chloromethyl)pyridine,[14] PhIO[15] and PhI^{18}O[16] were synthesized according to their literature procedures. 2,6-Lutidinium chloride was obtained by dropwise addition of 10 mL (10 mmol, 1 M in diethylether) HCl to a solution of 2,6-lutidine in 10 mL diethylether at 0 °C. After annealing to room temperature 15 mL hexane were added, and the supernatant was removed from the white precipitate formed by filtration. A second precipitation from diethylether/hexane followed by drying of the residue in vacuum led to 1.10 g (7.7 mmol, 77 %) of white 2,6-lutidinium chloride. ^{1}H NMR (300 MHz, CD$_3$CN): δ [ppm] = 2.82 (s, 7H, **CH$_3$ + NH**), 7.51 (d, $^3J(^1\text{H}, {}^1\text{H})$ = 7.9 Hz, 2H, **CH**), 8.15 (t, $^3J(^1\text{H}, {}^1\text{H})$ = 7.9 Hz, 1H, **CH**); ^{13}C{^{1}H} NMR (75 MHz, CD$_3$CN): δ [ppm] = 19.5 (**CH$_3$**), 125.6 (**CH^{Ar}**), 145.3 (**CH^{Ar}**), 154.4 (**C^{Ar}**); Anal. Calcd for C$_7$H$_{10}$NCl: C 58.54, H 7.02, N 9.75, Cl 24.69; found: C 58.67, H 6.92, N 9.71, Cl 24.34.

Synthesis of FurNeu. Based on a procedure published by *Buchwald* an co-workers[17] 2.24 g (5.3 mmol) 4,6-diiododibenzofuran, 2.30 g (12.8 mmol) HN((CH$_2$)$_2$N(CH$_3$)$_2$)(CH$_2$(2-py)), 166 mg (0.87 mmol) CuI, 4.56 g (21.4 mmol) K$_3$PO$_4$ and 1.2 mL (1.33 g, 21.4 mmol) ethylene glycol were suspended in 25 mL *iso*-propanol and the beige reaction mixture was stirred for 24 hours at 80 °C. After annealing to room temperature all volatile compounds were removed and the resulting brown residue was re-dissolved in 60 mL of CH$_2$Cl$_2$. The organic phase was washed with 75 mL of a saturated Na$_2$S$_2$O$_3$ solution. The organic layer was again separated and washed three times with 50 mL of H$_2$O while the aqueous phase was extracted four times each with 50 mL of CH$_2$Cl$_2$. The combined organic phases were dried over MgSO$_4$ and removal of the solvent in vacuum led to the isolation of a brown oil, which was further purified over a column of silica gel 60 (ethanol/CH$_2$Cl$_2$ 1:1, 1 vol% MeN(Et)$_2$, R$_f$ = 0.5). The resulting light brown viscous residue was dried for 3 days in vacuum and afterwards it was extracted with 15 mL of boiling hexane. The storage of the extract over 5 days at –30 °C led to the formation of a beige solid from which the solution was decanted and subsequent drying in vacuum gave 580 mg (1.1 mmol, 21 %) **FurNeu**. ^{1}H NMR (300 MHz, CD$_3$CN): δ [ppm] = 2.11 (s, 12H, **CH$_3$**), 2.48 (t, $^3J(^1\text{H}, {}^1\text{H})$ = 7.0 Hz, 4H, **CH$_2$**), 3.62 (t,

$^3J(^1H, ^1H) = 6.9$ Hz, 4H, **CH₂**), 4.80 (s, 4H, **CH₂**), 6.86 (dd, $^3J(^1H, ^1H) = 8.1$ Hz, $^4J(^1H, ^1H) =$ 1.1 Hz, 2H, **CH**), 7.12 (dd, $^3J(^1H, ^1H) = 7.5$ Hz, $^4J(^1H, ^1H) = 1.1$ Hz, 2H, **CH**), 7.13 (t, $^3J(^1H, ^1H) = 7.9$ Hz, 2H **CH**), 7.30 (*ps*-d, $J(^1H, ^1H) = 7.9$ Hz, 2H, **CH**), 7.39 (dd, $^3J(^1H, ^1H) = 7.7$ Hz, $^4J(^1H, ^1H) = 1.1$ Hz, 2H, **CH**), 7.57 (dt, $^3J(^1H, ^1H) = 7.7$ Hz, $^4J(^1H, ^1H) = 1.9$ Hz, 2H, **CH**), 8.46 (m, 2H, **CH**); ^{13}C{^{1}H} NMR (75 MHz, CD₃CN): δ [ppm] = 46.0 (**CH₃**), 51.0 (**CH₂**), 57.9 (**CH₂**), 58.5 (**CH₂**), 112.0 (**CH**^{Ar}), 115.6 (**CH**^{Ar}), 122.6 (**CH**^{Ar}), 122.8 (**CH**^{Ar}), 124.8 (**CH**^{Ar}), 126.5 (**C**^{Ar}), 136.7 (**C**^{Ar}), 137.2 (**CH**^{Ar}), 146.8 (**C**^{Ar}), 149.9 (**CH**^{Ar}), 160.5 (**C**^{Ar}). Anal. Calcd for C₃₂H₃₈N₆O: C 73.53, H 7.33, N 16.08; found: C 73.64, H 7.31, N 15.81; IR (KBr): $\widetilde{\nu}$ [cm^{-1}] = 3047 (w), 3006 (w), 2968 (m), 2938 (m), 2861 (m), 2823 (m), 2772 (m), 1654 (w), 1619 (m), 1592 (vs), 1568 (m), 1541 (w), 1499 (m), 1456 (m), 1427 (s), 1377 (w), 1343 (m), 1312 (w), 1263 (m), 1188 (m), 1164 (m), 1144 (s), 1092 (m), 1041 (m), 987 (w), 949 (w), 858 (w), 766 (s), 732 (m), 667 (w), 617 (w); MS (ESI/APCI, CH₃CN): m/z = 523.3407 (100 %, [**FurNeu** + H]$^+$, calcd 523.3185), 545.3124 (15 %, [**FurNeu** + Na]$^+$, calcd 545.3005).

Protonation of FurNeu. In an NMR experiment 2.8 mg (19.5 μmol) 2,6-lutidinium chloride were added to a solution of 5 mg (9.47 μmol) **FurNeu** in 0.5 mL acetonitrile-d₃. The resulting colorless reaction solution was investigated by means of ^{1}H NMR spectroscopy after 10 min. ^{1}H NMR (300 MHz, CD₃CN): δ [ppm] = 2.74 (s, 12H, **CH₃**), 3.30 (t, $^3J(^1H, ^1H)$ = 6.8 Hz, 4H, **CH₂**), 3.99 (t, $^3J(^1H, ^1H) = 6.8$ Hz, 4H, **CH₂**), 4.79 (s, 4H, **CH₂**), 7.16 – 7.24 (m, 4H, **CH**), 7.25 – 7.30 (m, 2H, **CH**), 7.54 (dd, $^3J(^1H, ^1H) = 7.7$ Hz, $^4J(^1H, ^1H) = 1.1$ Hz, 2H, **CH**), 7.64 (dt, $^3J(^1H, ^1H) = 7.7$ Hz, $^4J(^1H, ^1H) = 1.7$ Hz, 2H, **CH**), 8.63 (m, 2H, **CH**), 12.24 (br, 2H, N**H**). Moreover, the ^{1}H NMR spectrum contained the signal set caused by 2,6-lutidine (δ [ppm] = 2.43 (s, 6H, **CH₃**), 7.20 (d, $^3J(^1H, ^1H) = 7.7$ Hz, 2H, **CH**), 7.50 (t, $^3J(^1H, ^1H) = 7.7$ Hz, 1H, **CH**)). Slow diffusion of diethylether into the sample led to the formation of a micro-crystalline solid, which was identified as the dihydrochloride of the **FurNeu** molecule. IR (KBr): $\widetilde{\nu}$ [cm^{-1}] = 3044 (w), 3009 (w), 2961 (m), 2928 (w), 2854 (w), 2579 (m), 2515 (m), 2460 (s), 2418 (m), 1618 (m), 1592 (vs), 1570 (m), 1496 (s), 1473 (s), 1430 (vs), 1420 (s), 1391 (w), 1357 (m), 1262 (m), 1230 (w), 1187 (m), 1168 (m), 1138 (w), 1094 (w), 1067 (w), 1035 (w), 1018 (w), 971 (m), 859 (w), 778 (m), 752 (m), 739 (m); MS

(ESI, 100 V, CH$_3$CN): m/z = 262.1599 (30 %, [**FurNeu** + 2H]$^{2+}$, calcd 262.1626), 523.3154 (100 %, [**FurNeu** + H]$^+$, calcd 523.3154), 545.2971 (48 %, [**FurNeu** + Na]$^+$, calcd 545.3005).

Synthesis of [FurNeu](Cu$_2$(μ-Cl))(CuCl$_2$), 1. 20.0 mg (38.3 µmol) **FurNeu** and 11.4 mg (115.2 µmol) CuCl were dissolved in 5 mL thf and after 14 hours of stirring the volume of the resulting suspension was reduced in vacuum to 1 mL. Addition of 5 mL hexane to the reaction mixture caused the further precipitation of a pale yellow solid, which was filtered off. Drying of the residue in vacuum yielded in 18.6 mg (22.7 µmol, 59 %) **1**. Single crystals suitable for X-ray diffraction analysis were grown by slow diffusion of diethylether into a concentrated solution of **1** in acetonitrile. ^{1}H NMR (300 MHz, CD$_3$CN): δ [ppm] = 2.13 (s, 12H, **CH$_3$**), 2.47 (m, 4H, **CH$_2$**), 3.05 (m, 4H, **CH$_2$**), 4.71 (s, 4H, **CH$_2$**), 7.20 – 7.26 (m, 4H, **CH**), 7.35 – 7.40 (m, 4H, **CH**), 7.73 (dt, ^3J(^{1}H, ^{1}H) = 7.7 Hz, ^4J(^{1}H, ^{1}H) = 1.7 Hz, 2H, **CH**), 7.81 (dd, ^3J(^{1}H, ^{1}H) = 6.4 Hz, ^4J(^{1}H, ^{1}H) = 2.3 Hz, 2H, **CH**), 8.34 (m, 2H, **CH**); ^{13}C{^{1}H} NMR (75 MHz, CD$_3$CN): δ [ppm] = 48.3 (**CH$_3$**), 48.2 (**CH$_2$**), 58.7 (**CH$_2$**), 61.2 (**CH$_2$**), 116.7 (**CH^{Ar}**), 118.4 (**CH^{Ar}**), 124.6 (**CH^{Ar}**), 125.0 (2 x **CH^{Ar}**), 126.8 (**C^{Ar}**), 135.1 (**C^{Ar}**), 138.2 (**CH^{Ar}**), 148.9 (**C^{Ar}**), 150.1 (**CH^{Ar}**), 156.7 (**C^{Ar}**); Anal. Calcd for C$_{32}$H$_{38}$ N$_6$Cl$_3$Cu$_3$O: C 46.89, H 4.67, N 10.25, Cl 12.98; found: C 47.12, H 4.65, N 10.13, Cl 12.62; IR (KBr): $\tilde{\nu}$ [cm^{-1}] = 3054 (w), 3025 (w), 2956 (m), 2877 (s), 2829 (s), 2784 (m), 1625 (w), 1599 (vs), 1567 (w), 1498 (m), 1465 (s), 1437 (vs), 1364 (m), 1325 (m), 1284 (m), 1244 (m), 1192 (m), 1172 (m), 1153 (s), 1131 (w), 1035 (m), 972 (m), 942 (m), 899 (w), 845 (w), 779 (s), 732 (m), 575 (w), 476 (w); MS (ESI/APCI, CH$_3$CN): m/z = 523.3407 (75 %, [**FurNeu** + H]$^+$, calcd 523.3185), 585.2625 (100 %, [[**FurNeu**](Cu)]$^+$, calcd 585.2503), 674.1989 (16 %, [[**FurNeu**](Cu$_2$CN)]$^+$, calcd 674.1930), 683.1644 (8 %, [[**FurNeu**](Cu$_2$(μ-Cl))]$^+$, calcd 683.1587).

Synthesis of [FurNeu](CuCl$_2$)$_2$, 2. *Method A)* 10 mg (12.2 mmol) **[FurNeu]**(Cu$_2$(μ-Cl))(CuCl$_2$), **1**, were dissolved in 0.6 mL acetonitrile-d$_3$ and exposure to an atmosphere of air and O$_2$, respectively, led to a color change from pale yellow to green. Single crystals of **2**·1.5(CH$_3$CN) suitable for X-ray diffraction analysis were obtained by

slow evaporation of the solvent of the reaction solution. *Method B)* After stirring a green solution of 20 mg (38.3 µmol) **FurNeu** and 10.2 mg (76.5 µmol) $CuCl_2$ in 4 mL acetonitrile the volume was reduced in vacuum until a green precipitate began to form. The addition of 5 mL diethylether assisted the further precipitation and the colorless supernatant was removed by filtration. The resulting green residue was washed with 2 mL of hexane and subsequent drying in vacuum gave 23.5 mg (29.7 µmol, 78 %) solid **2**. X-ray diffraction analysis quality single crystals of **2**·2(CH_3CN) were grown by slow evaporation of the solvent from an acetonitrile solution of pure **2**. Anal. Calcd for $C_{32}H_{38}N_6Cl_4Cu_2O$: C 48.55, H 4.84, N 10.62, Cl 17.91; found: C 48.67, H 4.88, N 10.62, Cl 18.25; IR (KBr): $\tilde{\nu}$ [cm^{-1}] = 3435 (m), 3063 (w), 3021 (w), 2959 (m), 2925 (m), 2868 (m), 2843 (w), 1609 (s), 1493 (m), 1460 (s), 1448 (s), 1433 (vs), 1417 (s), 1384 (s), 1206 (m), 1283 (m), 1261 (m), 1247 (w), 1186 (m), 1161 (m), 1128 (m), 1095 (m), 1072 (m), 1053 (m), 1029 (s), 999 (m), 947 (m), 862 (m), 826 (m), 775 (s), 772 (s), 741 (m), 653 (w), 571 (w), 476 (w); MS (ESI, CH_3CN): m/z = 620.2103 (40 %, **[[FurNeu](CuCl)]**$^+$, calcd 620.2186), 753.0777 (100 %, **[[FurNeu](Cu₂Cl₃)]**$^+$, calcd 753.0959), 1408.2550 (1 %, **[[FurNeu](CuCl₂)[FurNeu](Cu₂Cl₃)]**$^+$, calcd 1408.2839), 1541.1228 (6 %, **[[FurNeu](Cu₂Cl₄)[FurNeu](Cu₂Cl₃)]**$^+$, calcd 1541.1612), 1942.6466 (0.2 %,**[([FurNeu](Cu₂Cl₄))₄[FurNeu](Cu₂Cl)]**$^{2+}$, calcd 1942.6939).

Synthesis of [FurNeu](Cu(NCCH₃))₂(OTf)₂, 3. A yellow solution of 20.0 mg (38.3 µmol) **FurNeu** and 28.8 mg (76.4 µmol) [Cu(NCCH₃)₄]OTf in 2 mL thf decolorized within 1 min. After additional 15 min the volume of the reaction mixture was reduced to 1 mL and 3 mL hexane were added. The beige precipitate formed was filtered off and drying of the solid in vacuum yielded in 24.3 mg (23.6 µmol, 61 %) **3**. ^{1}H NMR (300 MHz, CD_3CN): δ [ppm] = 1.96 (s, 6H, **CH₃**), 2.16 (s, br, 12H, **CH₃**), 2.50 (bt, 4H, **CH₂**), 3.11 (br, 4H, **CH₂**), 4.78 (br, 4H, **CH₂**), 7.27 – 7.38 (m, 4H, **CH**), 7.40 – 7.48 (m, 4H, **CH**), 7.84 – 7.93 (m, 4H, **CH**), 8.27 (br, 2H, **CH**); ^{13}C{^{1}H} NMR (75 MHz, CD_3CN): δ [ppm] = 48.1 (br, **CH₃**), 49.6 (**CH₂**), 58.8 (**CH₂**), 61.1 (**CH₂**), 117.5 (**CH**^{Ar}), 119.7 (**CH**^{Ar}), 125.1 (**CH**^{Ar}), 125.2 (**CH**^{Ar}), 125.4 (**CH**^{Ar}), 126.9 (**C**^{Ar}), 134.8 (**C**^{Ar}), 139.1 (**CH**^{Ar}), 148.8 (**C**^{Ar}), 150.0 (**CH**^{Ar}), 157.0 (**C**^{Ar}); Anal. Calcd for $C_{38}H_{44}N_8Cu_2F_6O_7S_2$: C 44.31, H 4.31, N 10.88, S 6.23; found: C

44.02, H 4.17, N 10.43, S 6.00; IR (KBr): $\widetilde{v}$ [cm^{-1}] = 3067 (w), 2987 (w), 2962 (w), 2928 (w), 2873 (w), 2845 (w), 2795 (m), 1602 (m), 1499 (w), 1465 (w), 1457 (m), 1440 (m), 1419 (m), 1340 (w), 1330 (m), 1273 (vs), 1223 (m), 1191 (w), 1154 (s), 1101 (w), 1084 (w), 1129 (vs), 981 (w), 969 (w), 943 (w), 845 (w), 789 (m), 771 (m), 755 (w), 731 (w), 695 (w), 637 (vs), 574 (m), 517 (m), 473 (w); **MS** (*Thermo Scientific* LTQ Ion Trap, ESI, CH$_3$CN): m/z = 324.2 (13 %, [**[FurNeu]**(Cu)$_2$]$^{2+}$, calcd 324.1), 435.2 (53 %, [**[FurNeu]**(Cu) - CH$_2$py - CH$_2$N(CH$_3$)$_2$]$^+$, calcd 435.1), 585.3 (100 %, [**[FurNeu]**(Cu)]$^+$, calcd 585.3), 797.1 (5%, [**[FurNeu]**(Cu)$_2$(OTf)]$^+$, calcd 797.1).

Protonation of [FurNeu](Cu(NCCH$_3$))$_2$(OTf)$_2$, 3. In an NMR experiment 1.4 mg (9.7 µmol) 2,6-lutidinium chloride were added to a solution of 5 mg (4.85 µmol) **[FurNeu]**(Cu(NCCH$_3$))$_2$(OTf)$_2$, **3**, in 0.5 mL acetonitrile-d$_3$. The resulting slightly yellow colored reaction solution was investigated by means of ^{1}H NMR spectroscopy after 10 min. ^{1}H NMR (300 MHz, CD$_3$CN): δ [ppm] = 1.96 (s, 6H, **CH$_3$**), 2.80 (s, br, 12H, **CH$_3$**), 3.15 (br, 4H, **CH$_2$**), 3.73 (br, 4H, **CH$_2$**), 4.63 (s, 4H, **CH$_2$**), 7.09 (d, ^3J(^{1}H, ^{1}H) = 7.7 Hz, 2H, **CH**), 7.22 (t, ^3J(^{1}H, ^{1}H) = 7.7 Hz, 2H, **CH**), 7.39 – 7.47 (m, 2H, **CH**, overlaps with one signal caused by 2,6-lutidine), 7.57 – 7.68 (m, 2H, **CH**, overlaps with one signal caused by 2,6-lutidine), 7.91 (dt, ^3J(^{1}H, ^{1}H) = 7.7 Hz, ^4J(^{1}H, ^{1}H) = 1.7 Hz, 2H, **CH**),   8.63 (d, br, 2H, **CH**), 12.04 (br, 2H, N**H**). Moreover, the ^{1}H NMR spectrum contained the signal set caused by 2,6-lutidine.

Synthesis of [FurNeu](Cu)$_2$(OTf)$_4$, 4. 20 mg (38.3 µmol) **FurNeu** and 27.7 mg (76.5 µmol) Cu(OTf)$_2$ were dissolved in 2 mL acetonitrile, and the resulting blue solution was stirred for 10 min. Subsequent addition of 8 mL diethylether led to the formation of an oily blue residue that was isolated by filtration. Drying of the residue in vacuum, followed by re-dissolution in 3 mL thf and the addition of 10 mL hexane led to the formation of a finely dispersed precipitate. After filtration the solid was completely dissolved in 0.5 mL acetonitrile. Slow diffusion of diethylether into this solution led to the growth of blue single crystals (quality only sufficient for the determination of the atom connectivity by X-ray diffraction analysis), from which the supernatant was decanted, and subsequent drying in vacuum gave 23.7 mg (18.5 µmol) of crystalline **4**. ^{19}F NMR (282 MHz, CD$_3$CN): δ [ppm] = -78.06 (s); Anal.

Calcd for $C_{36}H_{38}N_6Cu_2F_{12}O_{13}S_4$: C 34.70, H 3.07, N 6.74, S 10.29; found: C 34.78, H 3.26, N 6.84, S 10.15; IR (KBr): $\tilde{\nu}$ [cm^{-1}] = 3089 (w), 3044 (w), 2963 (w), 2869 (w), 1654 (m), 1617 (m), 1483 (m), 1466 (m), 1458 (m), 1437 (m), 1420 (m), 1279 (s), 1242 (vs), 1224 (vs), 1165 (vs), 1126 (m), 1095 (m), 1075 (m), 1058 (m), 1030 (vs), 948 (w), 864 (m), 793 (m), 772 (m), 739 (m), 637 (vs), 574 (m), 517 (m); MS (ESI, 100V, CH$_3$CN): m/z = 367.6016 (100 %, [[**FurNeu**](Cu)(OTf)$_2$H]$^+$, calcd 585.2503), 734.1944 (10 %, [[**FurNeu**](Cu)(OTf)]$^+$, calcd 734.2017), 884.11556 (71 %, [[**FurNeu**](Cu)(OTf)$_2$H]$^+$, calcd 844.1616), 1095.0322 (6 %, [[**FurNeu**](Cu)$_2$(OTf)$_3$]$^+$, calcd 1095.0454); UV/Vis (CH$_3$CN, 2 mM): λ_{max} (ε) = 612 nm (260 M^{-1}cm^{-1}).

Access to [FurNeu](Cu$_2$(μ-O))(OTf)$_2$, 5. *Method A)* 6.2 mg (6 µmol) **[FurNeu]**(Cu(NCCH$_3$))$_2$(OTf)$_2$, **3**, were dissolved in 2 mL acetonitrile. Through the resulting colorless solution dry O$_2$ was bubbled for 10 s and after 20 min of vigorous stirring the reaction mixture was investigated spectroscopically. MS (ESI, 100V, CH$_3$CN): m/z = 262.1643 (76 %, [[**FurNeu**] + 2H]$^{2+}$, calcd 262.1626), (332.0825 (1 %, [[**FurNeu**](Cu$_2$(μ-O))]$^{2+}$, calcd 332.0919), 362.0941 (22 %, [[**FurNeu**](Cu$_2$(μ-O)) + CH$_3$COOH]$^{2+}$, calcd 362.1024), 523.3200 (30 %, [[**FurNeu**] + H]$^+$, calcd 523.3185), 585.2458 (100 %, [[**FurNeu**](Cu)]$^+$, calcd 585.2503), 872.1548 (13 %, [[**FurNeu**](Cu$_2$(μ-O))(OTf) + CH$_3$CN + H$_2$O]$^+$, calcd 872.1734); UV/Vis (CH$_3$CN, 2 mM): λ_{max} = 644 nm. Further UV/Vis measurements were performed at a concentration of 0.1 mM. *Method B)* After dissolution of 10.0 mg (9.71 µmol) **[FurNeu]**(Cu(NCCH$_3$))$_2$(OTf)$_2$, **3**, in 0.5 – 2 mL acetonitrile or acetonitrile-d$_3$ 2.1 mg (9.55 µmol) PhIO were added. The resulting pale green suspension turned into a dark green solution in the course of the following 20 min under vigorous stirring, which was investigated spectroscopically. If necessary the solvent was removed prior the spectroscopic studies. ^{1}H NMR (300 MHz, CD$_3$CN): δ [ppm] = 2.14 (s, br, 12H, C**H**$_3$), 2.48 (bt, 4H, C**H**$_2$), 3.09 (br, 4H, C**H**$_2$), 4.78 (br, 4H, C**H**$_2$), 7.27 – 7.37 (m, 4H, C**H**), 7.41 – 7.47 (m, 4H, C**H**), 7.83 – 7.95 (m, 4H, C**H**), 8.25 (ps-d, , J(^{1}H, ^{1}H) = 4.7 Hz, 2H, C**H**). In some cases the ^{1}H NMR spectra contained the signal sets of the by-products PhI (δ [ppm] = 7.17 (ps-t, 2H, C**H**), 7.39 (ps-t, 1H, C**H**), 7.75 (m, 2H, C**H**)) and acetonitrile (δ [ppm] = 1.96 (s, C**H**$_3$)), respectively. IR (KBr, Figure S12): $\tilde{\nu}$ [cm^{-1}] = 2964 (m),

2874 (w), 2803 (w), 1658 (m), 1625 (w), 1603 (m), 1568 (m), 1496 (w), 1469 (m), 1438 (m), 1419 (m), 1369 (w), 1263 (vs), 1224 (m), 1151 (s), 1103 (m), 1057 (w), 1030 (vs), 981 (w), 971 (w), 943 (w), 898 (w), 872 (w), 844 (w), 790 (m), 756 (w), 738 (m), 690 (w), 674 (w), 637 (s), 574 (m), 517 (m), 476 (w), 456 (w), 419 (w); IR (CH_3CN): Figure S11; MS (*Thermo Scientific* LTQ Ion Trap, ESI, CH_3CN): m/z = 332.1 (13 %, [**[FurNeu]**$(Cu_2(\mu$-O$))$]$^{2+}$, calcd 332.1), 435.2 (100 %, [**[FurNeu]**(Cu) - CH_2py - $CH_2N(CH_3)_2$]$^+$, calcd 435.1), 494.3 (48 %, [**[FurNeu]**(Cu) - CHpy]$^+$, calcd 494.2), 585.3 (82 %, [**[FurNeu]**(Cu)]$^+$, calcd 585.3), 706.1 (37 %, [**[FurNeu]**$(Cu)_2(OH)(CH_3CN)$]$^+$, calcd 706.2), 797.1 (5%, [**[FurNeu]**$(Cu)_2(OTf)$]$^+$, calcd 797.1); MS (ESI, 100V, CH_3CN): m/z = 332.0864 (3 %, [**[FurNeu]**$(Cu_2(\mu$-O$))$]$^{2+}$, calcd 332.0919), 362.0980 (100 %, [**[FurNeu]**$(Cu_2(\mu$-O$))$ + CH_3COOH]$^{2+}$, calcd 362.1024), 458.0529 (4 %, [**[FurNeu]**$(Cu_2)(OAc)(OTf)$]$^{2+}$, calcd 458.0876), 585.2438 (15 %, [**[FurNeu]**(Cu)]$^+$, calcd 585.2503), 644.2604 (4 %, [**[FurNeu]**(Cu)(OAc)]$^+$, calcd 644.2631); UV/Vis (CH_3CN, 2mM): λ_{max} (ε) = 644 nm (140 $M^{-1}cm^{-1}$). A similar UV/Vis experiment employing 2 eq. PhIO led to the same spectroscopic features and intensities. Further UV/Vis measurements were performed at a concentration of 0.1 mM.

Access to [FurNeu]$(Cu_2(\mu$-^{18}O$))$(OTf)$_2$, 5^{18O}. *Method A)* A solution of 4.1 mg (4 µmol) **[FurNeu]**$(Cu(NCCH_3))_2(OTf)_2$, **3**, in 0.5 mL acetonitrile was placed in an screw-cap *Young* NMR tube, which was evacuated and cooled to -60 °C. Subsequently, the tube containing the frozen solution was exposed to a $^{18}O_2$ atmosphere. Annealing to room temperature gave a dark green solution, which was investigated with the aid of mass spectrometry. MS (ESI, 100V, CH_3CN): m/z = 262.1622 (24 %, [**[FurNeu]** + 2H]$^{2+}$, calcd 262.1626), 363.0943 (63 %, [**[FurNeu]**$(Cu_2(\mu$-^{18}O$))$ + CH_3COOH]$^{2+}$, calcd 363.1050), 585.2396 (100 %, [**[FurNeu]**(Cu)]$^+$, calcd 585.2503), 674.1726 (13 %, [**[FurNeu]**(Cu_2CN)]$^+$, calcd 674.1930), 874.1551 (14 %, [**[FurNeu]**$(Cu_2(\mu$-^{18}O$))(OTf$ + CH_3CN + H_2O]$^+$, calcd 874.1785). *Method B)* As described above for the reaction employing PhIO **[FurNeu]**$(Cu(NCCH_3))_2(OTf)_2$, **3**, was reacted with 2.1 mg (9.46 µmol) PhI^{18}O instead. IR (KBr, Figure S12): The IR spectrum of **[FurNeu]**$(Cu_2(\mu$-^{18}O$))$(OTf)$_2$, 5^{18O}, was identical to the one detected for **[FurNeu]**$(Cu_2(\mu$-^{16}O$))$(OTf)$_2$, **5**. IR (CH_3CN): Figure S11; MS (*Thermo Scientific* LTQ FT Ultra, ESI, CH_3CN): m/z = 333.0833 (3 %, [**[FurNeu]**$(Cu_2(\mu$-^{18}O$))$]$^{2+}$, calcd 333.0944),

363.0946 (100 %, [[**FurNeu**]($Cu_2(\mu$-^{18}O)) + CH_3COOH]$^{2+}$, calcd 363.1050), 585.2373 (28 %, [[**FurNeu**](Cu)]$^+$, calcd 585.2503). MS^2 (*Thermo Scientific* LTQ FT Ultra, ESI, CH_3CN, [[**FurNeu**]($Cu_2(\mu$-^{18}O)) + CH_3COOH]$^{2+}$, m/z = 363): m/z = 324.0770 (100 %, [363 - CH_3COOH - ^{18}O]$^{2+}$, calcd 324.0944), 333.0861 (13 %, [363 - CH_3COOH]$^{2+}$, calcd 333.0944, mixture with [[**FurNeu**]($Cu_2(\mu$-^{16}O))]$^{2+}$ (332.0811)), 363.0972 (6 %, [[**FurNeu**]($Cu_2(\mu$-^{18}O)) + CH_3COOH]$^{2+}$, calcd 363.1050).

[FurNeu]($Cu_2(\mu$-O))(OTf)$_2$, 5, in the Presence of Carboxylic Acids. To a solution of 4.1 mg (4 µmol) **[FurNeu]**($Cu(NCCH_3)$)$_2$(OTf)$_2$, **3**, in 0.3 mL acetonitrile 1-2 droplets of an approximately 0.1 % solution of the corresponding carboxylic acid dissolved in acetonitrile were added, and subsequently O_2 was bubbled through the resulting solution for 30 s. After 20 min of vigorous stirring the reaction mixture was investigated by means of mass spectrometry. MS (ESI, 100V, CH_3CN): *formic acid:* m/z = 262.1655 (33 %, [[**FurNeu**] + 2H]$^{2+}$, calcd 262.1626), 355.0875 (9 %, [[**FurNeu**]($Cu_2(\mu$-O)) + HCOOH]$^{2+}$, calcd 355.0946), 585.2467 (100 %, [[**FurNeu**](Cu)]$^+$, calcd 585.2503); *acetic acid:* m/z = 262.1659 (42 %, [[**FurNeu**] + 2H]$^{2+}$, calcd 262.1626), 322.6332 (8 %, [[**FurNeu**](Cu) + CH_3COOH]$^{2+}$, calcd 322.6352), 362.0970 (54 %, [[**FurNeu**]($Cu_2(\mu$-O)) + CH_3COOH]$^{2+}$, calcd 362.1024), 585.2466 (100 %, [[**FurNeu**](Cu)]$^+$, calcd 585.2503), 644.2569 (12 %, [[**FurNeu**](Cu) + CH_3COOH]$^+$, calcd 644.2631); *propionic acid:* m/z = 262.1650 (62 %, [[**FurNeu**] + 2H]$^{2+}$, calcd 262.1626), 369.1024 (14 %, [[**FurNeu**]($Cu_2(\mu$-O)) + C_2H_5COOH]$^{2+}$, calcd 369.1102), 585.2434 (100 %, [[**FurNeu**](Cu)]$^+$, calcd 585.2503).

In order to investigate the behavior of **[FurNeu]($Cu_2(\mu$-O))(OTf)$_2$, 5**, in the presence of acetic acid by ^1H NMR as well as UV/Vis spectroscopy to the corresponding acetonitrile solutions of **5** (NMR: 10 mM in acetonitrile-d_3, UV/Vis: 2 mM or 0.1 mM) 1.2 eq. of HOAc (0.175 M in acetonitrile) were added. The results are shown in the Figures S15-S19.

Decomposition of [FurNeu]($Cu_2(\mu$-O))(OTf)$_2$, 5. To a solution of 15.4 mg (14.95 µmol) **[FurNeu]**($Cu(NCCH_3)$)$_2$(OTf)$_2$, **3**, in 1 mL acetonitrile 3.3 mg (14.95 µmol) PhIO were added and the resulting pale green suspension turned into a dark green solution in the course of the following 20 min under vigorous stirring. Storage of the solution for at least 3 days at

room temperature led to the formation of 0.3 mg (0.97 µmol, 7 %) crystalline [Cu(picoloyl)$_2$], which was identified by means of single-crystal X-ray diffraction analysis and IR spectroscopy. IR (KBr): $\widetilde{\nu}$ [cm^{-1}] = 1640 (s), 1604 (m), 1570 (w), 1473 (w), 1448 (w), 1353 (m), 1309 (w), 1285 (m), 1244 (m), 1172 (w), 1150 (w), 1130 (w), 1096 (w), 1047 (w), 985 (w), 851 (w), 825 (w), 775 (w), 765 (w), 713 (w), 694 (w), 662 (w), 544 (w), 458 (w), 418 (w). The analytical data determined are in agreement with those previously reported.[12] Furthermore, single crystals of [Cu(picoloyl)$_2$] could be grown by the slow evaporation of the solvent of a solution of 10.0 mg (9.71 µmol) **[FurNeu]**(Cu(NCCH$_3$))$_2$(OTf)$_2$, **3**, in 1 mL acetonitrile under aerobic conditions. The cell parameters matched those of [Cu(picoloyl)$_2$].

Reaction of [FurNeu](Cu$_2$(μ-O))(OTf)$_2$, 5, with PPh$_3$. After dissolving 10.0 mg (9.71 µmol) **[FurNeu]**(Cu(NCCH$_3$))$_2$(OTf)$_2$, **3**, and 2.1 mg (9.55 µmol) PhIO in 0.5 mL acetonitrile-d$_3$ the reaction mixture was vigorously stirred for 20 min, and the complete conversion to **5** and PhI was ensured by ^{1}H NMR spectroscopy. To the resulting green solution 12.7 mg (48.54 µmol) PPh$_3$ were added and after further 3 hours 3.76 mg (9.71 µmol) [n-Bu$_4$N]PF$_6$ as an internal standard The conversion to (O)PPh$_3$ (8 %, with respect to the amount of **3** employed) was determined by ^{31}P NMR spectroscopy. The yield was determined from two replicate runs and is given with an accuracy of ±1 %. ^{31}P NMR (121.5 MHz, CD$_3$CN, d1 = 4 s, ns = 10.500): δ [ppm] = 27.50.

Catalytic Oxidative Coupling of 2,4-Di-*tert*-butylphenol, DTBP, to 3,3',5,5'-Tetra-*tert*-butyl 2,2'-biphenol, TBBP, and Further Oxidation to 2,4,7,9-Tetra-*tert*-butyloxepino[2,3-b]benzofuran, TBOBF, via 3,3',5,5'-tetra-*tert*-butyl 2,2'-diphenoquinone, TBDQ, in Presence of [FurNeu](Cu$_2$(μ-O))(OTf)$_2$, 5. After dissolving 10.0 mg (9.71 µmol) **[FurNeu]**(Cu(NCCH$_3$))$_2$(OTf)$_2$, **3**, and 2.1 mg (9.55 µmol) PhIO in 0.5 mL acetonitrile-d$_3$ the reaction mixture was vigorously stirred for 20 min. To the resulting green solution 4.0 mg (19.39 µmol) DTBP were added and after further 3 hours of stirring 3.73 µL (3.36 mg, 48.54 µmol) dimethylformamide were added as an internal standard to the light brown solution, which was then investigated by NMR spectroscopy. The conversion to

56 % TBBP (based on the amount of DTBP employed) was determined with the help of ^{1}H NMR spectroscopy. The subsequent exposure of the reaction mixture to an atmosphere of O_2 led to a color change of the solution from light brown over purple to green within one hour. Afterwards the complete conversion of DTBP and TBBP, respectively, to TBOBF was again confirmed by ^{1}H NMR spectroscopy. A control experiment in the absence **3** showed that PhIO itself is also capable to mediate the oxidative coupling to give TBBP (22 % yield after 3 hours) and for that reason the complete conversion of **3** and PhIO giving **5** and PhI was ensured by ^{1}H NMR spectroscopy prior to the addition of DTBP. Yields were determined from at least two replicate runs and are given with an accuracy of ±1 %. The isolation of single crystalline TBOBF was achieved by storing the reaction solution at 4 °C. *TBBP:* ^{1}H NMR (300 MHz, CD$_3$CN): δ [ppm] = 1.31 (s, 18H, C(**CH$_3$**)$_3$), 1.42 (s, 18H, C(**CH$_3$**)$_3$), 7.01 (d, $^4J(^1$H, ^{1}H) = 2.4 Hz, 2H, C**H**), 7.37 (d, $^4J(^1$H, ^{1}H) = 2.4 Hz 2H, C**H**); ^{13}C{^{1}H} NMR (75 MHz, CD$_3$CN): δ [ppm] = 30.0 (C(**CH$_3$**)), 31.8 (C(**CH$_3$**)), 34.9 (**C**(CH$_3$)), 35.7 (**C**(CH$_3$)), 124.8 (**CH**^{Ar}), 126.5 (**C**^{Ar}), 126.8 (**CH**^{Ar}), 137.6 (**C**^{Ar}), 143.7 (**C**^{Ar}), 150.8 (**C**^{Ar}); *TBOBF:* ^{1}H NMR (300 MHz, CD$_3$CN): δ [ppm] = 1.20 (s, 9H, C(**CH$_3$**)$_3$), 1.25 (s, 9H, C(**CH$_3$**)$_3$), 1.35 (s, 9H, C(**CH$_3$**)$_3$), 1.44 (s, 9H, C(**CH$_3$**)$_3$), 5.61 (s, 1H, C**H**), 6.50 (s, 1H, C**H**), 7.20 (d, $^4J(^1$H, ^{1}H) = 1.9 Hz, 1H, C**H**), 7.40 (d, $^4J(^1$H, ^{1}H) = 1.9 Hz 1H, C**H**). ^{13}C{^{1}H} NMR (75 MHz, CD$_3$CN): δ [ppm] = 28.2 (C(**CH$_3$**)), 30.0 (C(**CH$_3$**)), 30.0 (C(**CH$_3$**)), 32.0 (C(**CH$_3$**)), 34.9 (**C**(CH$_3$)), 35.5 (**C**(CH$_3$)), 36.4 (**C**(CH$_3$)), 37.8 (**C**(CH$_3$)), 98.7 (**C**^{Ar}), 108.3 (**CH**^{Ar}), 113.8 (**CH**^{Ar}), 114.3 (**CH**^{Ar}), 118.5 (**CH**^{Ar}), 128.0 (**C**^{Ar}), 134.2 (**C**^{Ar}), 146.5 (**C**^{Ar}), 146.8 (**C**^{Ar}), 147.1 (**C**^{Ar}), 155.3 (**C**^{Ar}), 165.1 (**C**^{Ar}); Anal. Calcd for C$_{28}$H$_{40}$O$_2$: C 82.30, H 9.87; found: C 82.22, H 9.47; IR (KBr): $\tilde{\nu}$ [cm^{-1}] = 2962 (vs), 2930 (s), 2907 (s), 2869 (m), 1652 (m), 1634 (m), 1600 (m), 1578 (m), 1560 (m), 1542 (w), 1479 (m), 1459 (m), 1422 (m), 1393 (m), 1363 (m), 1340 (w), 1280 (m), 1252 (w), 1243 (w), 1201 (w), 1106 (w), 1083 (m), 1061 (s), 1048 (m), 1024 (w), 1009 (w), 912 (w), 878 (w), 863 (w), 854 (m), 827 (m), 798 (w), 780 (w), 760 (w), 711 (m), 672 (m), 648 (w); MS (APCI, CH$_3$CN): m/z = 409.3115 (100 %, [TBOBF + H]$^+$, calcd 409.3101); UV/Vis (CH$_3$CN, 2 mM) TBBP $\rightarrow$ [**TBDQ**]$\rightarrow$ TBOBF: λ_{max} (ε) = 573 nm (260 M^{-1}cm^{-1}).

Catalytic Oxidative Coupling of DTBP to TBBP and Further Oxidation TBOBF, via TBDQ in Presence of [FurNeu](Cu(NCCH$_3$))$_2$(OTf)$_2$, 3, and O$_2$. Exposure of a solution consisting of **[FurNeu]**(Cu(NCCH$_3$))$_2$(OTf)$_2$, **3**, and DTBP dissolved in 0.5 – 4 mL acetonitrile to an atmosphere of O$_2$ led to a color change from pale yellow over purple to green within the reaction time of 3 hours. The reactions were monitored by means of NMR spectroscopy and several yields of TBBP and TBOBF (based on the amount of DTBP) were determined by ^{1}H NMR spectroscopy. The results of a variety of experiments received are summarized in Table S4 and Scheme S5. Upon employment of stoichiometric and sub-stoichiometric amounts of O$_2$, respectively, the ^{1}H NMR spectrum of the reaction mixture additionally exhibited a set of signals similar to the one caused by **3**: ^{1}H NMR (300 MHz, CD$_3$CN): δ [ppm] = 1.96 (s, 6H, **CH$_3$**), 2.16 (s, br, 12H, **CH$_3$**), 2.48 (bt, 4H, **CH$_2$**), 3.11 (br, 4H, **CH$_2$**), 4.78 (br, 4H, **CH$_2$**), 7.27 – 7.38 (m, 4H, **CH**), 7.40 – 7.45 (m, 4H, **CH**), 7.83 – 7.91 (m, 4H, **CH**), 8.27 (d, br, J(^{1}H, ^{1}H) = 4.7 Hz, 2H, **CH**).

Catalytic Oxidation of TBBP to TBOBF, via TBDQ in Presence of [FurNeu](Cu(NCCH$_3$))$_2$(OTf)$_2$, 3, and O$_2$. In an NMR experiment 10.0 mg (9.71 µmol) **[FurNeu]**(Cu(NCCH$_3$))$_2$(OTf)$_2$, **3**, and 8 mg (19.42 µmol) TBBP were dissolved in 0.5 mL acetonitrile-d$_3$ and subsequently exposed to dioxygen. The investigation of the reaction mixture after 14 hours by ^{1}H NMR spectroscopy ensured the complete conversion to TBOBF.

Reactivity of [FurNeu](Cu)$_2$(OTf)$_4$, 4, towards DTBP. To a blue solution consisting of 5.0 mg (9.71 µmol) **FurNeu** and 7.0 mg (19.42 µmol) Cu(OTf)$_2$ with 0.5 mL acetonitrile-d$_3$ as the solvent 4.0 mg (19.39 µmol) DTBP were added. The reaction mixture decolorized within 3 hours and subsequently a yield of 50 % TBBP (based on DTBP) was determined by means of ^{1}H NMR spectroscopy. Moreover, the signal set originating from protonated **[FurNeu]**(Cu(NCCH$_3$))$_2$(OTf)$_2$, **3**, (see above) was detected. In the course of the monitoring the reaction with the help of UV/Vis spectroscopy the addition of 2 eq. DTBP to a 2 mM solution of **4** in acetonitrile caused the decrease of the characteristic absorption band at 612 nm.

Crystal Structure Determinations.

All data collections were performed at 100 K with a STOE IPDS 2T diffractometer. In all cases Mo-Kα radiation (λ = 0.71073 Å) was used; radiation source was a sealed tube generator with graphite monochromator. The structures were solved by direct methods (SHELXS-97)[19] and refined by full-matrix least squares procedures based on F2 with all measured reflections (SHELXL-97).[19] All non-hydrogen atoms were refined anisotropically. Hydrogen atoms were introduced in their idealized positions and refined as riding. Crystallographic data for the structures reported in this paper have been deposited at the Cambridge Crystallographic Data Centre as supplementary publication no. CCDC 936970 (for **1**), 936971 (for **2**·2(CH$_3$CN)), 936972 (for [Cu(picoloyl)$_2$]), and 936973 (for TBOBF). These data can be obtained free of charge from The Cambridge Crystallographic Data Center via www.ccdc.cam.ac.uk/data_request/cif.

^{1}H NMR spectrum of [FurNeu](Cu$_2$(μ-Cl))(CuCl$_2$), 1.
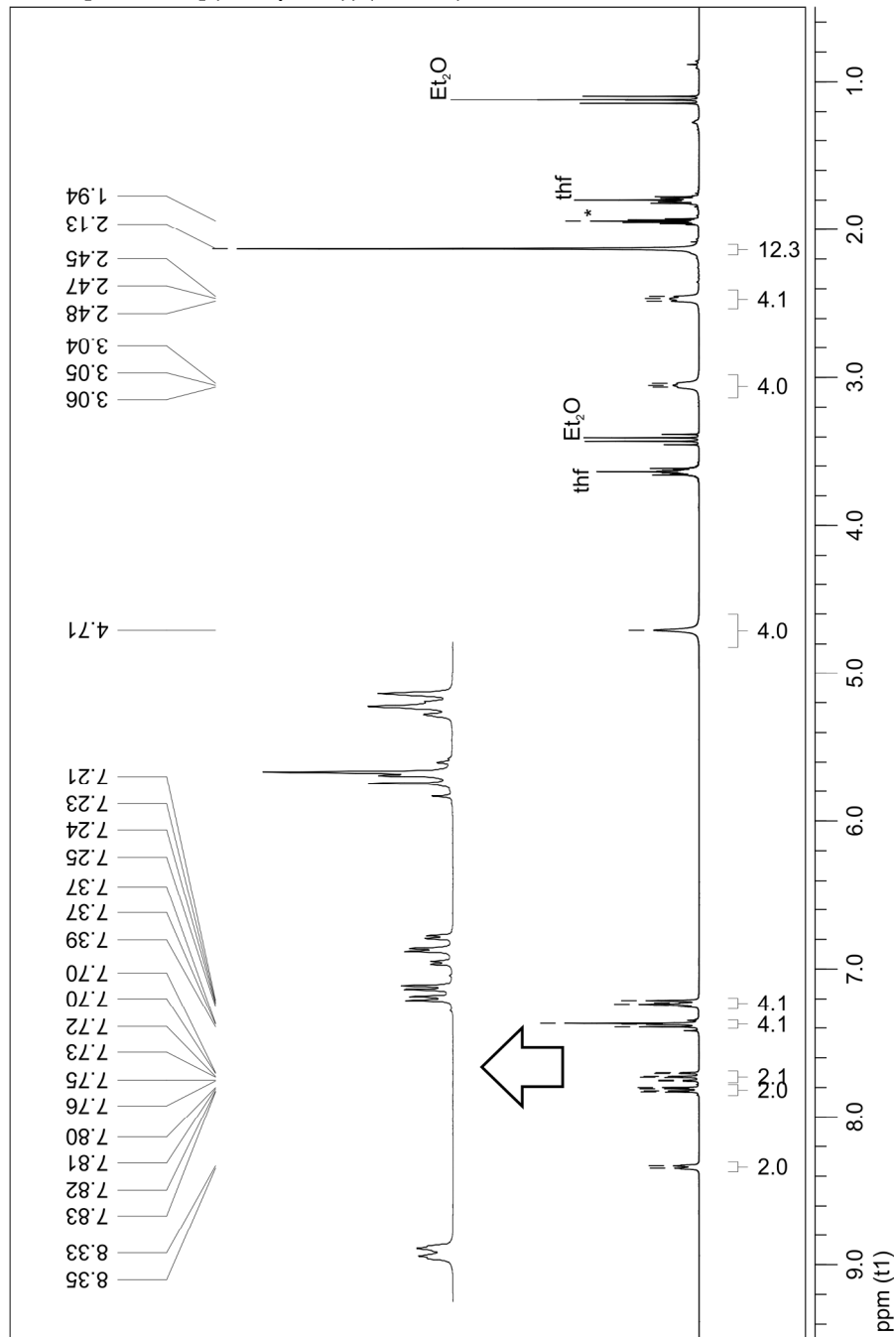
Figure S1. ^{1}H NMR spectrum of a solution of **[FurNeu]**(Cu$_2$(μ-Cl))(CuCl$_2$), **1**, with acetonitrile-d$_3$ as the solvent. The signal of the residual protons of the solvent is marked with an asterisk. The thf as well as Et$_2$O signals derive from impurities of the solvent used.

Discussion of the compounds [FurNeu](CuCl$_2$)$_2$, 2, and [FurNeu](Cu)$_2$(OTf)$_4$, 4.

[FurNeu](CuCl$_2$)$_2$, 2. Yellow solutions of **1** in acetonitrile changed their color to green within seconds upon exposure to air or dioxygen. NMR investigations pointed to the formation of a paramagnetic product containing Cu^{II} ions (Scheme S1). Single crystals of this product were grown by slow evaporation of the solvent from the reaction mixture at room temperature, and through an X-ray diffraction analysis **[FurNeu]**(CuCl$_2$)$_2$, **2**, could be clearly identified as one oxidation product of **1** (Figure S1). Considering the different Cu/Cl ratios in **1** (3:3) and **2** (2:4) only a maximum yield of 75 % based on the amount of **1** employed is to be expected. However, it was not possible to clarify the identity of the remaining equivalents of copper and **FurNeu**, respectively.
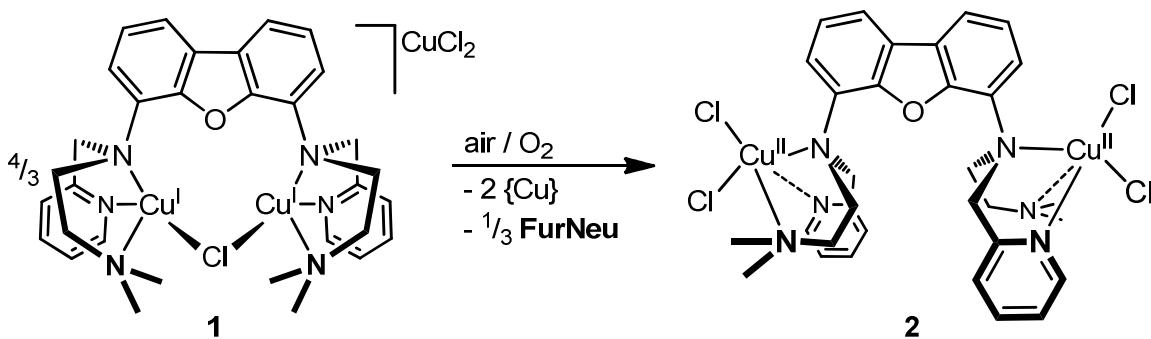
Scheme S1. Synthesis of **[FurNeu]**(CuCl$_2$)$_2$, **2**, by oxidation of **[FurNeu]**(Cu$_2$(μ-Cl))(CuCl$_2$), **1**, with air and dioxygen, respectively.
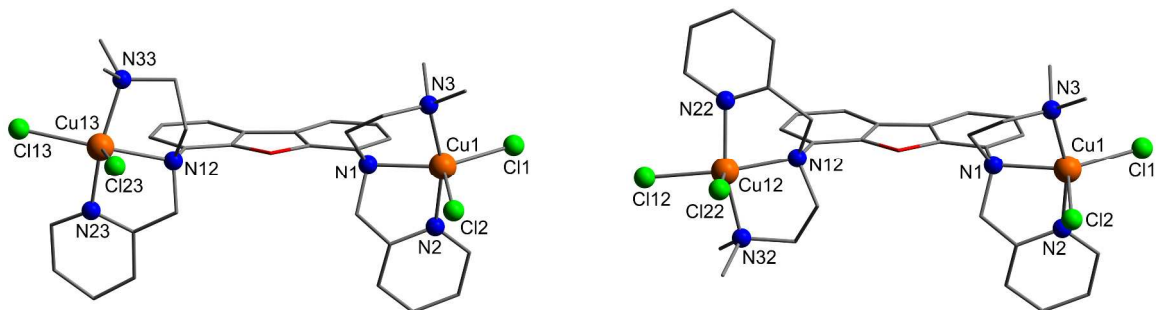
Figure S2. Molecular structure of **[FurNeu]**(CuCl$_2$)$_2$, **2**, co-crystallized with 1.5 molecules of acetonitrile. Due to the disorder of one N_3-binding pocket the *cis-* (left side) and *trans-* configuration of the pyridylmethyl and dimethylaminoethylene units coexist in a 65:35 ratio within the crystal. Single crystals were grown by slow evaporation of the solvent from the reaction mixture after oxygenation of a solution of **1** in acetonitrile without any further purification steps at room temperature. All hydrogen atoms and solvent molecules were omitted for clarity. Due to the disorder mentioned above the quality of the data set was not sufficient to allow for a detailed discussion of the structural parameters of **2**·1.5(CH$_3$CN). However, the molecular structure shown reflects unambiguously the atom connectivity of **2**·1.5(CH$_3$CN). Space group: Pbca, a = 15.6837(5) Å, b = 17.1953(5) Å, c = 28.2942(8) Å, α = 90°, β = 90°, γ = 90°, V = 7630.5(4) Å^3.

Alternatively, **2** is also easily accessible by the reaction between **FurNeu** and two equivalents of CuCl$_2$ in acetonitrile as the solvent with a yield of 78 % (Scheme S2). **2** was fully characterized and again single crystals suitable for X-ray diffraction analysis could be grown by slow evaporation of the solvent from a concentrated solution of pure **2** in acetonitrile (Figure S3).

Scheme S2. Direct synthesis of **[FurNeu]**(CuCl$_2$)$_2$, **2**.
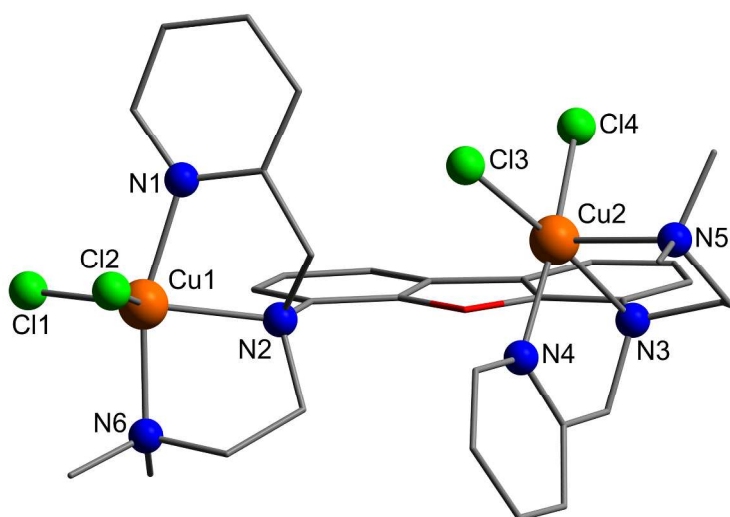
Figure S3. Molecular structure of **[FurNeu]**(CuCl$_2$)$_2$, **2**, co-crystallized with 2 molecules of acetonitrile. The corresponding single crystals were grown by slow evaporation of the solvent from a concentrated solution of pure **2** in acetonitrile at room temperature. All hydrogen atoms and solvent molecules were omitted for clarity. Selected bond lengths [Å] and angles [°]:Cu1–Cl1 2.2979(6), Cu1–Cl2 2.3789(7), Cu1–N1 2.021(2), Cu1–N2 2.1465(19), Cu1–N6 2.0377(19), Cu2–Cl3 2.2763(6), Cu2–Cl4 2.2530(7), Cu2–N3 2.1894(18), Cu2–N4 2.032(2), Cu2–N5 2.257(2), Cl1–Cu1–Cl2 116.41(3), Cl1–Cu1–N1 98.66(6), Cl2–Cu1–N1 87.90(6), Cl1–Cu1–N2 133.76(5), Cl1–Cu1–N6, 96.81(6), Cl2–Cu1–N2 109.72(5), Cl2–Cu1–N6 94.11(6), N1–Cu1–N2 79.38(7), N1–Cu1–N6 161.59(8), N2–Cu1–N6 82.72(8), Cl3–Cu2–Cl4 94.20(2), Cl3–Cu2–N3 175.24(6), N3–Cu2–N5 83.95(7), Cl3–Cu2–N4 94.13(6), Cl3–Cu2–N5 98.28(5), Cl4–Cu2–N3 89.38(6), Cl4–Cu2–N4 163.35(6), Cl4–Cu2–N5 102.72(6), N3–Cu2–N4 81.62(8), N4–Cu2–N5 90.30(8).

Due to the absence of by-products conditions regarding the crystallization process were slightly different and this might explain that the molecular structure determined differs in the orientation of the $CuCl_2$-fixing N_3-binding units. In contrast to the molecular structure of **1** (Figure 2, main text) none of the structures of **2** determined exhibit a bridging chloride ligand between the copper centers.

[FurNeu](Cu)$_2$(OTf)$_4$, 4. The reaction of **FurNeu** and two equivalents of copper(II) triflate in acetonitrile as the solvent was accompanied by an immediate color change of the reaction mixture to deep blue. Subsequent work up gave **[FurNeu]**(Cu)$_2$(OTf)$_4$, **4**, in 50 % yield and it was fully characterized (Scheme S3). NMR investigations pointed to a paramagnetic product, and the EPR spectrum of a solution of **4** in acetonitrile (13 mM) contained the anticipated copper(II) pattern. The UV/Vis spectrum of a solution of **4** in acetonitrile (2 mM) showed intensive absorptions in the range of 200 to 400 nm originating from the ligand backbone and an additional broad absorption band with a maximum at 612 nm ($\varepsilon = 260$ M^{-1} cm^{-1}, Figure 3, grey line, main text). The latter signal can be assigned to a copper(II) d-d transition.

Single crystals suitable for single-crystal X-ray diffraction analysis could be grown by slow diffusion of diethylether into a concentrated solution of **4** in acetonitrile. **4** crystallizes as a dimer in which two copper(II) ions are bridged by triflate anions in an intermolecular fashion. The coordination spheres of the copper ions are completed by one acetonitrile ligand and one N_3-based binding unit each. Within a monomeric entity of **4** the two copper centers are orientated away from each other. Due to the presence of heavily disordered non-coordinating triflate anions the quality of the data determined was not sufficient to allow for a detailed discussion of the binding parameters of (**4**(NCCH$_3$)$_2$)$_2$. However, the molecular structure shown in Figure S4 reflects unambiguously the atom connectivity within single crystalline (**4**(NCCH$_3$)$_2$)$_2$. Drying of (**4**(NCCH$_3$)$_2$)$_2$ in vacuum led to the complete loss of the acetonitrile molecules bound to the copper centers giving **[FurNeu]**(Cu)$_2$(OTf)$_4$, **4**.
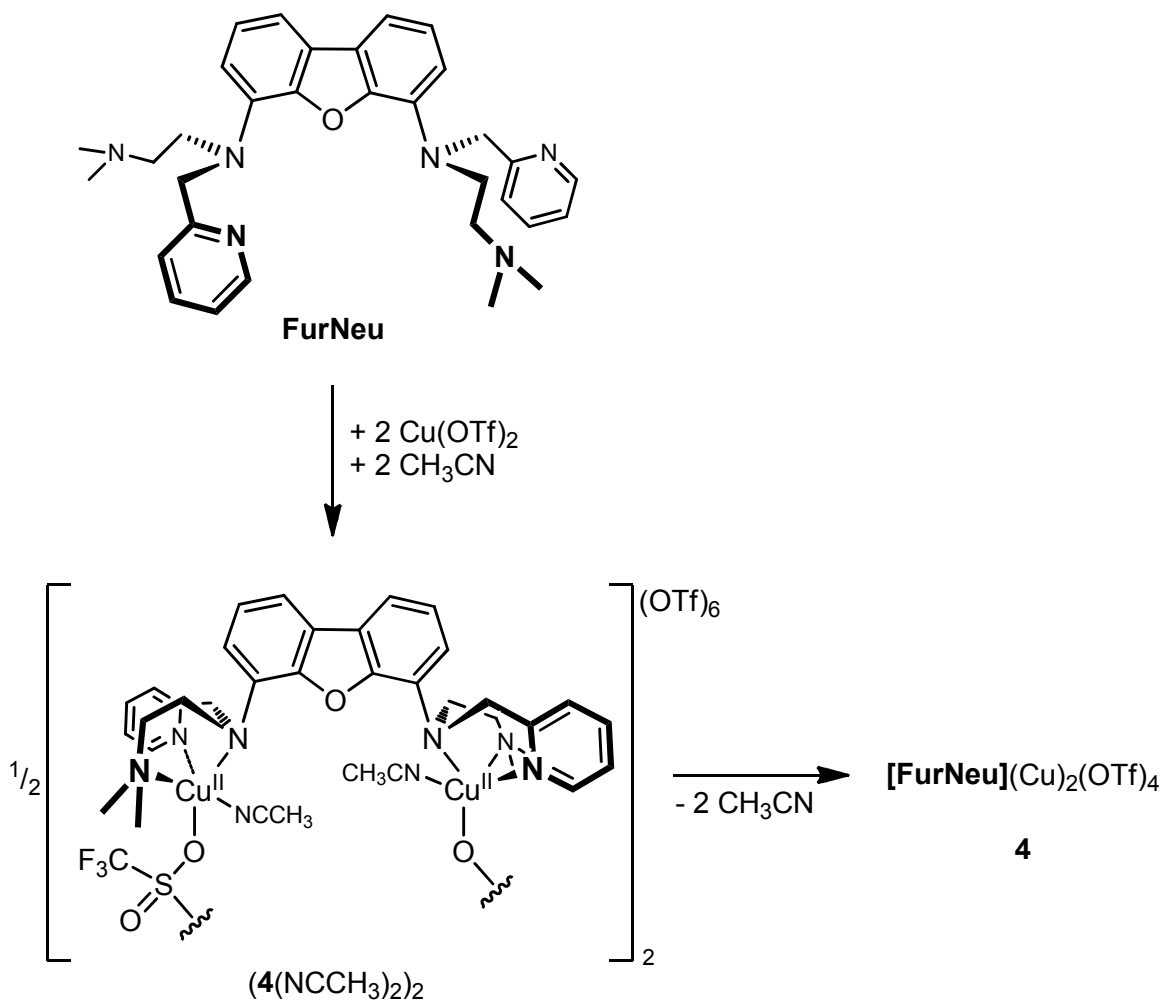
Scheme S3. Synthesis of **[FurNeu]**(Cu)$_2$(OTf)$_4$, **4**.
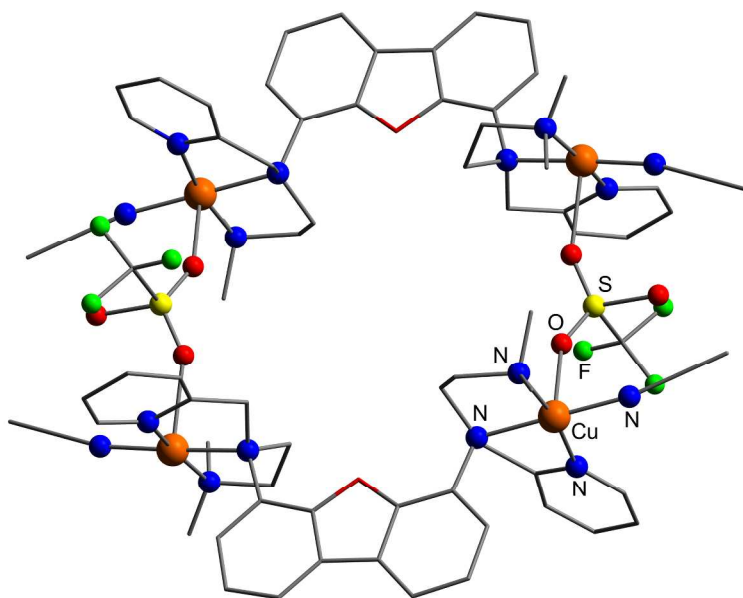
Figure S4. Molecular structure of {[**FurNeu**](Cu)$_2$(OTf)$_4$(NCCH$_3$)$_2$}$_2$, (**4**(NCCH$_3$)$_2$)$_2$. The corresponding single crystals were grown by slow diffusion of diethylether into a concentrated solution of **4** in acetonitrile at room temperature. All hydrogen atoms and non-coordinating triflate anions were omitted for clarity. Due to a heavy disorder of the non-coordinated triflate anions the quality of the data set was not sufficient to allow for a detailed discussion of the structural parameters of (**4**(NCCH$_3$)$_2$)$_2$. However, the molecular structure shown reflects unambiguously the atom connectivity of (**4**(NCCH$_3$)$_2$)$_2$. Space group: Pnnm, a = 13.9263(6) Å, b = 17.0261(8) Å, c = 24.0273(10) Å, α = 90°, β = 90°, γ = 90°, V = 5697.1(4) Å^3. (Further information: The complex (**4**(NCCH$_3$)$_2$)$_2$ consists of two triflate anions per Cu atom: two triflate anions lay on a special position and one on a general position. One of the triflate anions on special positions is coordinating to a Cu atom and its symmetry equivalent forming a dimer complex molecule. The other two triflate anions are not coordinated. Both molecules lying on special positions are disordered: the triflate anion within the complex dimer is disordered over two positions; the uncoordinated triflate anion is heavily disordered.)

Table S1. Crystallographic data and experimental parameters for the crystal structure analyses of **1**, **2**·2(CH$_3$CN), [Cu(picoloyl)$_2$] and TBOBF.

	1	**2**·2(CH$_3$CN)
synonym	**[FurNeu]**(Cu$_2$(μ-Cl))(CuCl$_2$)	**[FurNeu]**(CuCl$_2$)$_2$ ·2(CH$_3$CN)
empirical formula	C$_{32}$H$_{38}$Cl$_3$Cu$_3$N$_6$O	C$_{36}$H$_{44}$Cl$_4$Cu$_2$N$_8$O
weight / g mol^{-1}	819.68	873.69
temperatur / K	100(2)	100(2)
crystal system	triclinic	monoclinic
space group	P-1	P21/c
a / Å	10.1796(5)	15.4999(7)
b / Å	11.8184(6)	13.4120(4)
c / Å	14.1121(6)	20.0419(10)
α / °	94.264(4)	90
β / °	101.559(4)	114.396(3)
γ / °	95.426(4)	90
V / Å^3	1648.30(14)	3794.4(3)
Z, density / g cm^{-3}]	2, 1.651	4, 1.529
μ(Mo-K_α) / mm^{-1}	2.198	1.445
F$_{000}$	836	1800
Θ range / °	2.39 - 29.22	4.64 - 27.50
completeness to Θ [%]	99.9	98.1
collected reflexions	30444	29832
unique reflexions	8888	8547
GoF F^2	1.049	1.017
R indices [I>2σ(I)]	R1 = 0.0293, wR2 = 0.0742	R1 = 0.0388, wR2 = 0.0720
R indices (all data)	R1 = 0.0357, wR2 = 0.0764	R1 = 0.0583, wR2 = 0.0755
Δρmax / Δρmin / e Å^{-3}	0.716 / -0.601	0.651 / -1.047

|	[Cu(picoloyl)$_2$]	TBOBF
synonym	[Cu(picoloyl)$_2$]	TBOBF
empirical formula	C$_{12}$H$_8$CuN$_2$O$_4$	C$_{28}$H$_{40}$O$_2$
weight / g mol^{-1}	307.75	408.62
temperatur / K	100(2)	100(2)
crystal system	monoclinic	triclinic
space group	P2$_1$/c	P-1
a / Å	3.6979(2)	11.4816(4)
b / Å	11.9769(5)	13.0484(5)
c / Å	11.8765(6)	19.0797(6)
α / °	90	73.875(3)
β / °	91.093(4)	74.082(3)
γ / °	90	67.477(3)
V / Å^3	525.91(4)	2490.75(15)
Z, density / g cm^{-3}]	2, 1.943	4, 1.090
μ(Mo-K_α) / mm^{-1}	2.089	0.066
F$_{000}$	310	896
Θ range / °	2.42 - 29.50	3.26 to 29.50
completeness to Θ [%]	99.9	99.8
collected reflexions	9172	37127
unique reflexions	1463	13829
GoF F^2	0.946	1.093
R indices [I>2σ(I)]	R1 = 0.0247, wR2 = 0.0621	R1 = 0.0533, wR2 = 0.1556
R indices (all data)	R1 = 0.0314, wR2 = 0.0631	R1 = 0.0722, wR2 = 0.1636
$\Delta\rho$max / $\Delta\rho$min / e Å^{-3}	0.354 / -0.825	0.394 / -0.302

UV/Vis Spectroscopy.
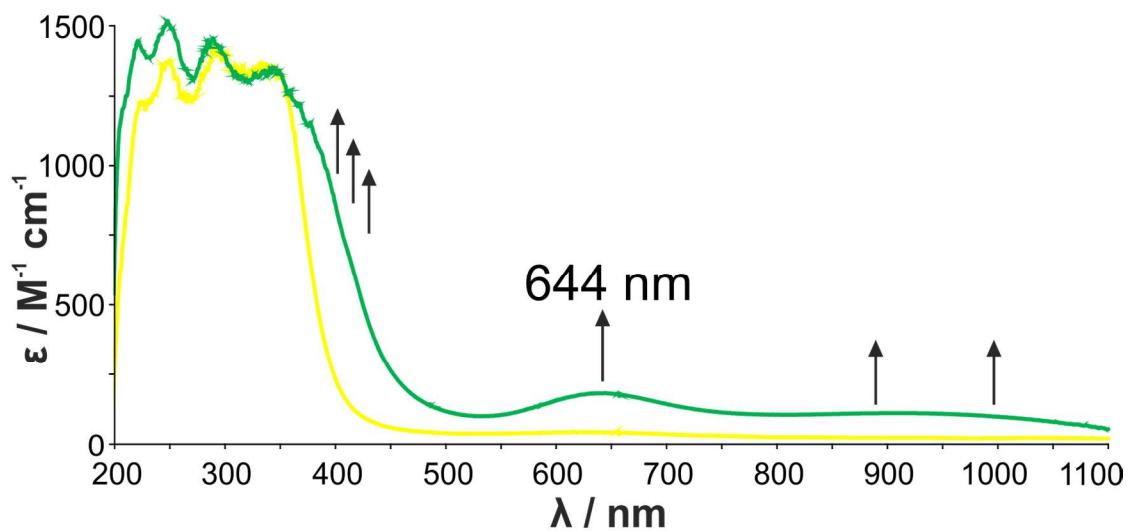
Figure S5. UV/Vis spectra of a solution of **[FurNeu]**(Cu(NCCH$_3$))$_2$(OTf)$_2$, **3**, dissolved in acetonitrile (2 mM) before (yellow line) and 10 min after the reaction with 1 eq. PhIO (green line, for the corresponding UV/Vis spectra recorded under diluted conditions (0.1 mM) including a dilution series see Figures S6-S8).
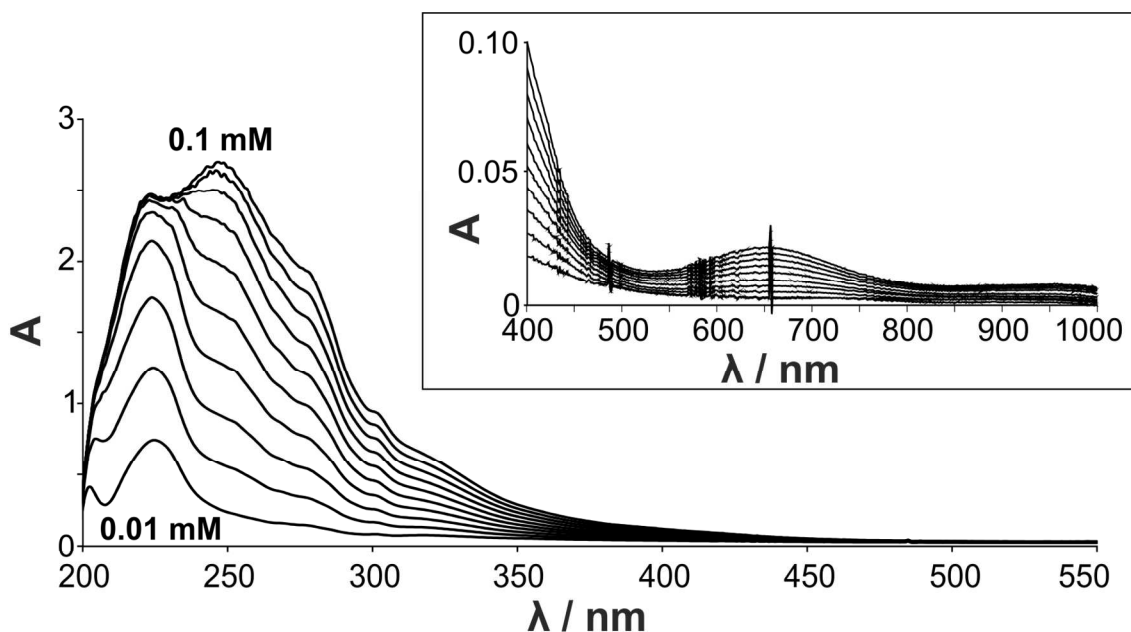
Figure S6. UV/Vis spectra of a dilution series of acetonitrile solutions (0.1, 0.09, 0.08, 0.07, 0.06, 0.05. 0.04, 0.03, 0.02, 0.01 mM) of **[FurNeu]**$(Cu_2(\mu\text{-}O))(OTf)_2$, **5**, which was generated via the reaction of **[FurNeu]**$(Cu(NCCH_3))_2(OTf)_2$, **3**, and PhIO.
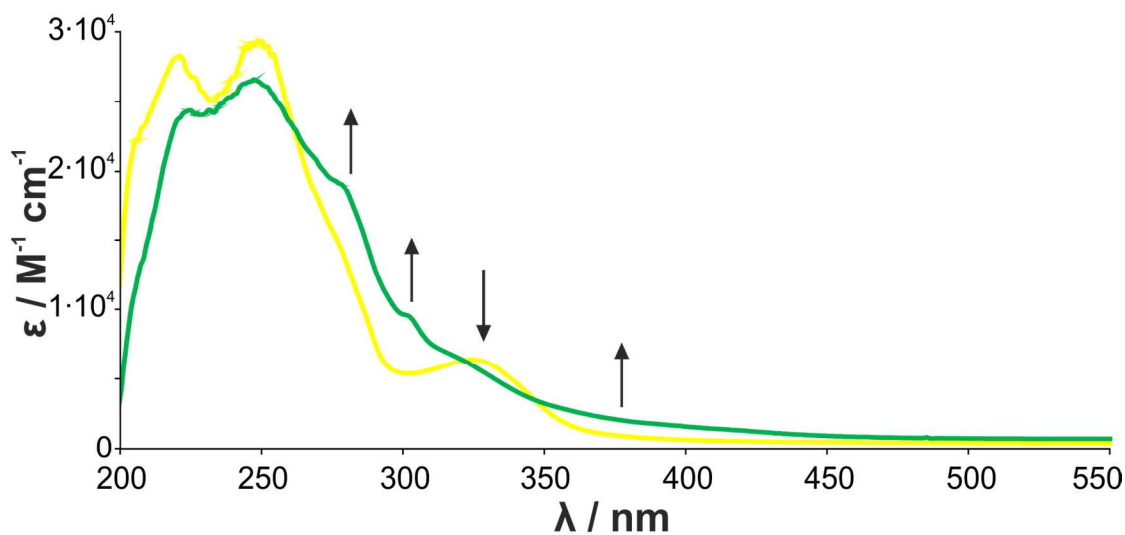
Figure S7. UV/Vis spectra of a solution of **[FurNeu]**$(Cu(NCCH_3))_2(OTf)_2$, **3**, dissolved in acetonitrile (0.1 mM) before (yellow line) and after reaction with PhIO (green line).
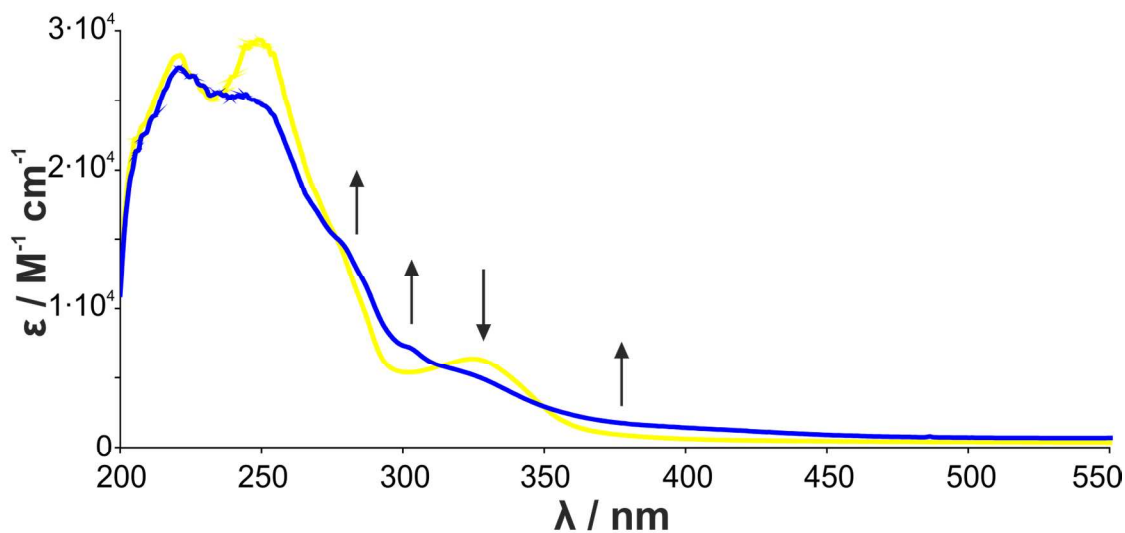
Figure S8. UV/Vis spectra of a solution of **[FurNeu]**(Cu(NCCH$_3$))$_2$(OTf)$_2$, **3**, dissolved in acetonitrile (0.1 mM) before (yellow line) and after reaction with O$_2$ (blue line).
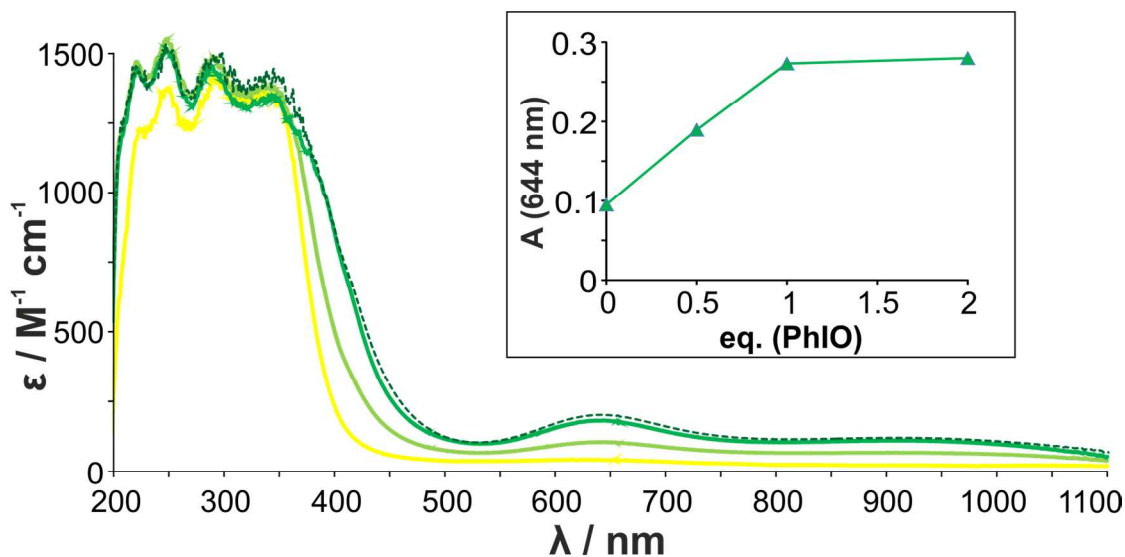
Figure S9. UV/Vis spectra of a solution of **[FurNeu]**(Cu(NCCH$_3$))$_2$(OTf)$_2$, **3**, dissolved in acetonitrile (2 mM) before (yellow line) and 10 min after the reaction with 0.5 eq. PhIO (pale green line), 1 eq. PhIO (green line) and 2 eq. PhIO (dotted dark green line), respectively. The inset shows the plot of absorbance of the 644 nm band vs. the number of equivalents of PhIO (0, 0.5, 1.0, and 2.0 eq.) employed.
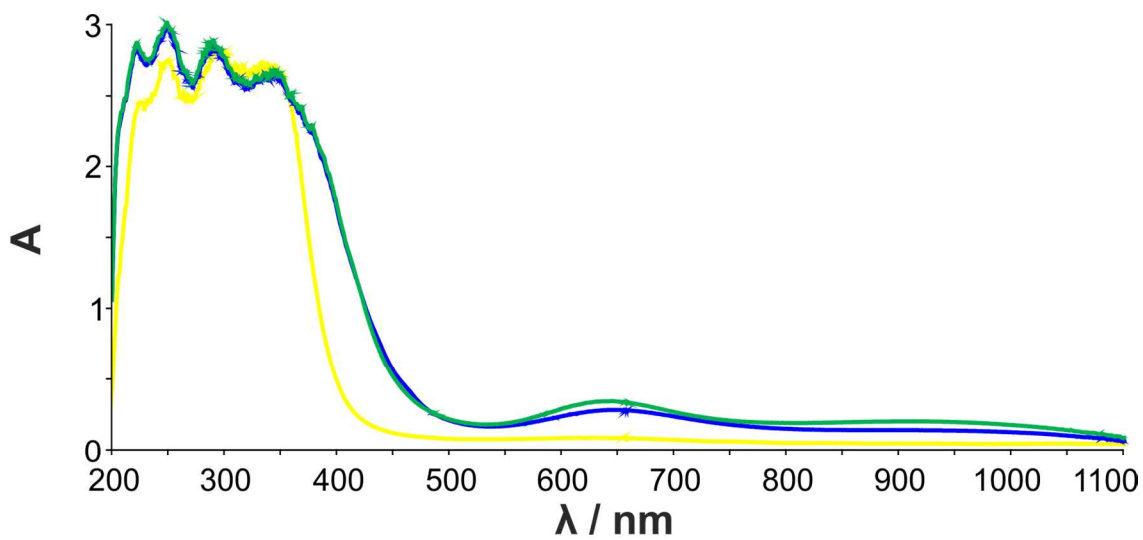
Figure S10. UV/Vis spectrum of a solution of **[FurNeu]**(Cu(NCCH$_3$))$_2$(OTf)$_2$, **3**, dissolved in acetonitrile (2 mM, yellow line) and comparison of the spectra obtained 20 min after the reaction with O$_2$ (blue line) and 10 min after the reaction with 1 eq. PhIO (green line), respectively.

IR Spectroscopy.
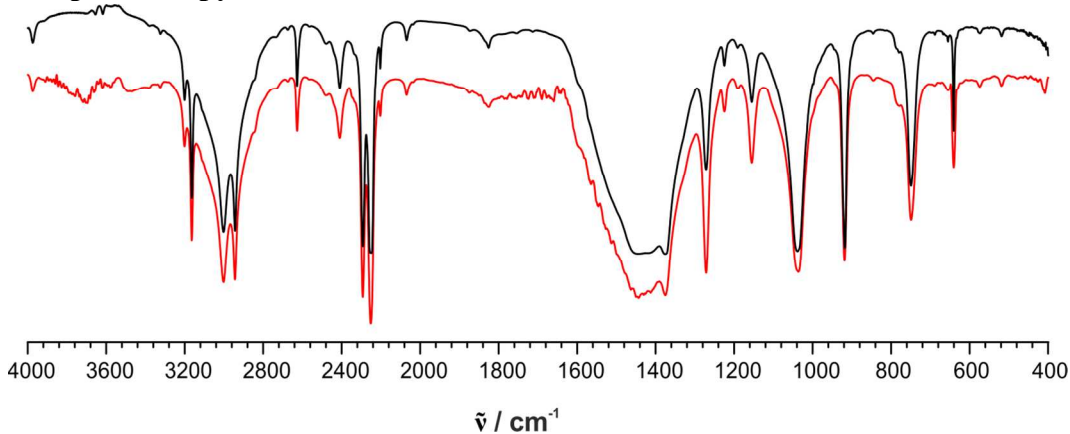
Figure S11. IR spectra of solutions (3 mM) of **[FurNeu]**$(Cu(NCCH_3))_2(OTf)_2$, **3**, dissolved in acetonitrile after the reaction with 1 eq. PhI[16]O (black line) and 1 eq. PhI[18]O (red line), respectively. No isotope sensitive signals were observed.
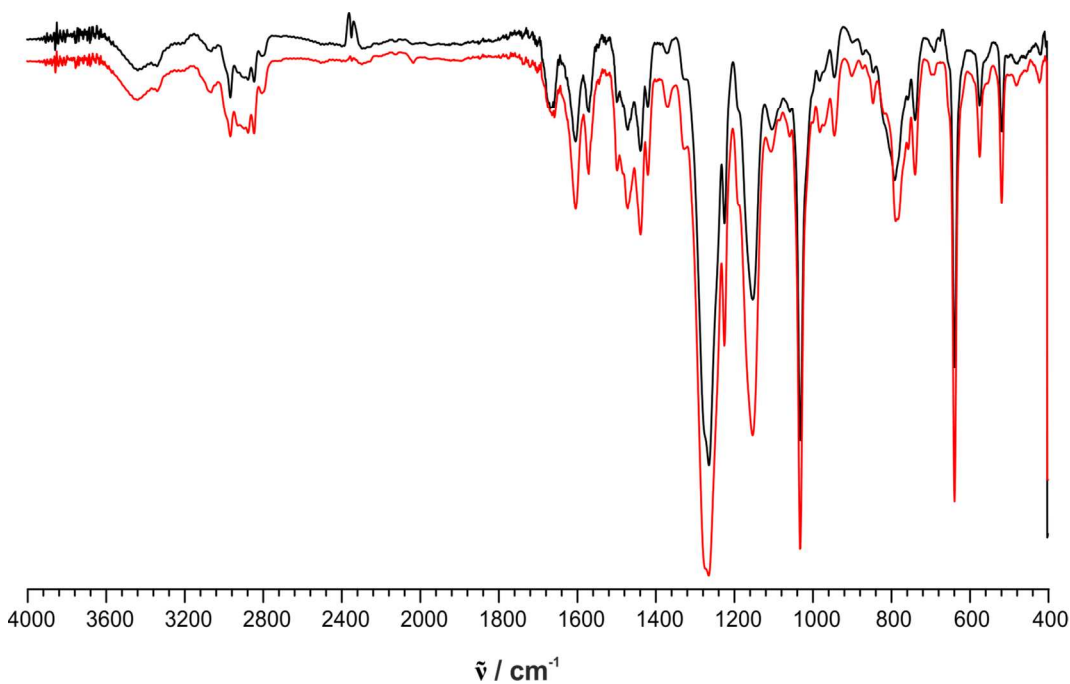
Figure S12. IR spectra (KBr pellets) of the solids obtained after evaporation of all volatiles from reaction mixtures composed of **[FurNeu]**$(Cu(NCCH_3))_2(OTf)_2$, **3**, and 1 eq. PhI[16]O (black line) or 1 eq. PhI[18]O (red line) in acetonitrile solution. No isotope sensitive signals were observed.

Mass Spectrometry.
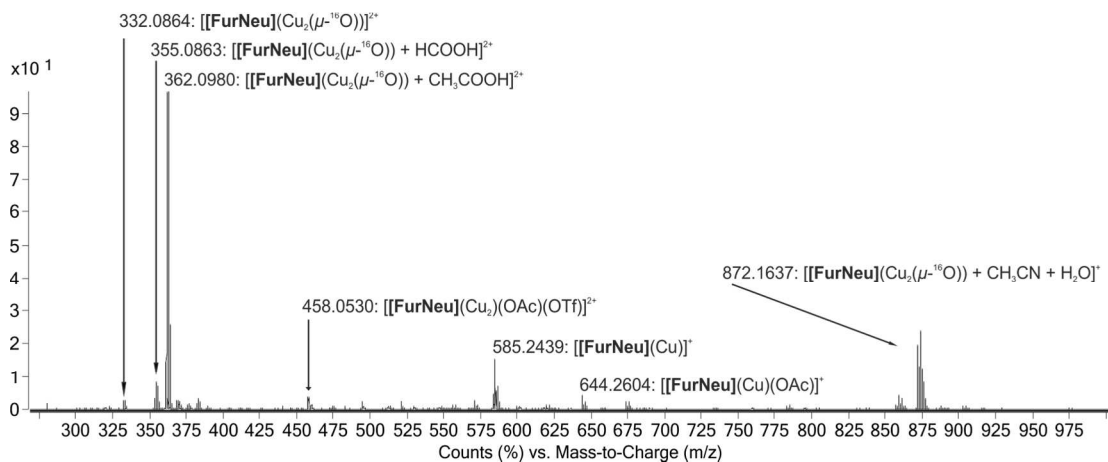
Figure S13. HR-ESI mass spectrum of a solution of **[FurNeu]**$(Cu_2(\mu\text{-}^{16}O))(OTf)_2$, **5**, in acetonitrile. In this case **5** was generated via the reaction of **3** with PhI^{16}O.
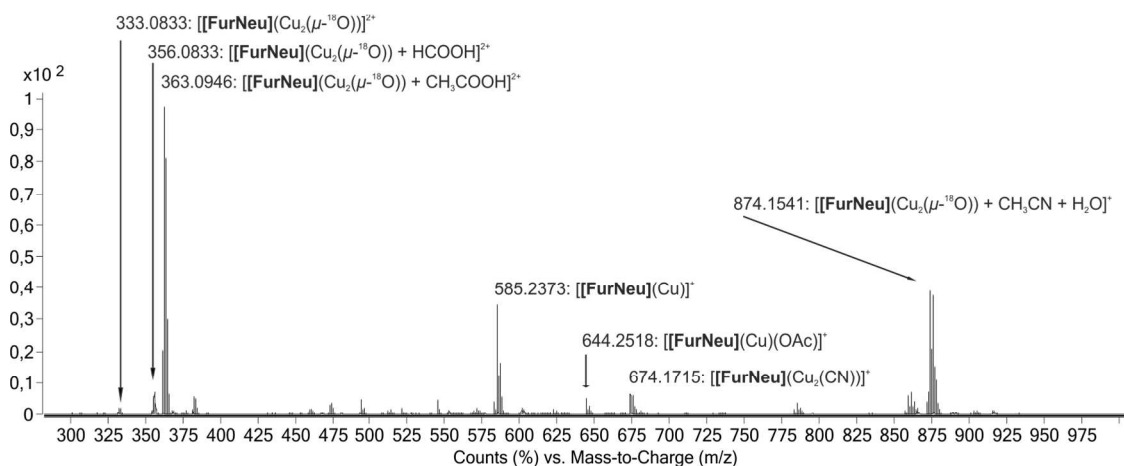
Figure S14. HR-ESI mass spectrum of a solution of **[FurNeu]**$(Cu_2(\mu\text{-}^{18}O))(OTf)_2$, **5^{18O}**, in acetonitrile. In this case **5^{18O}** was generated via the reaction of **3** with PhI^{18}O.

Protonation Studies.
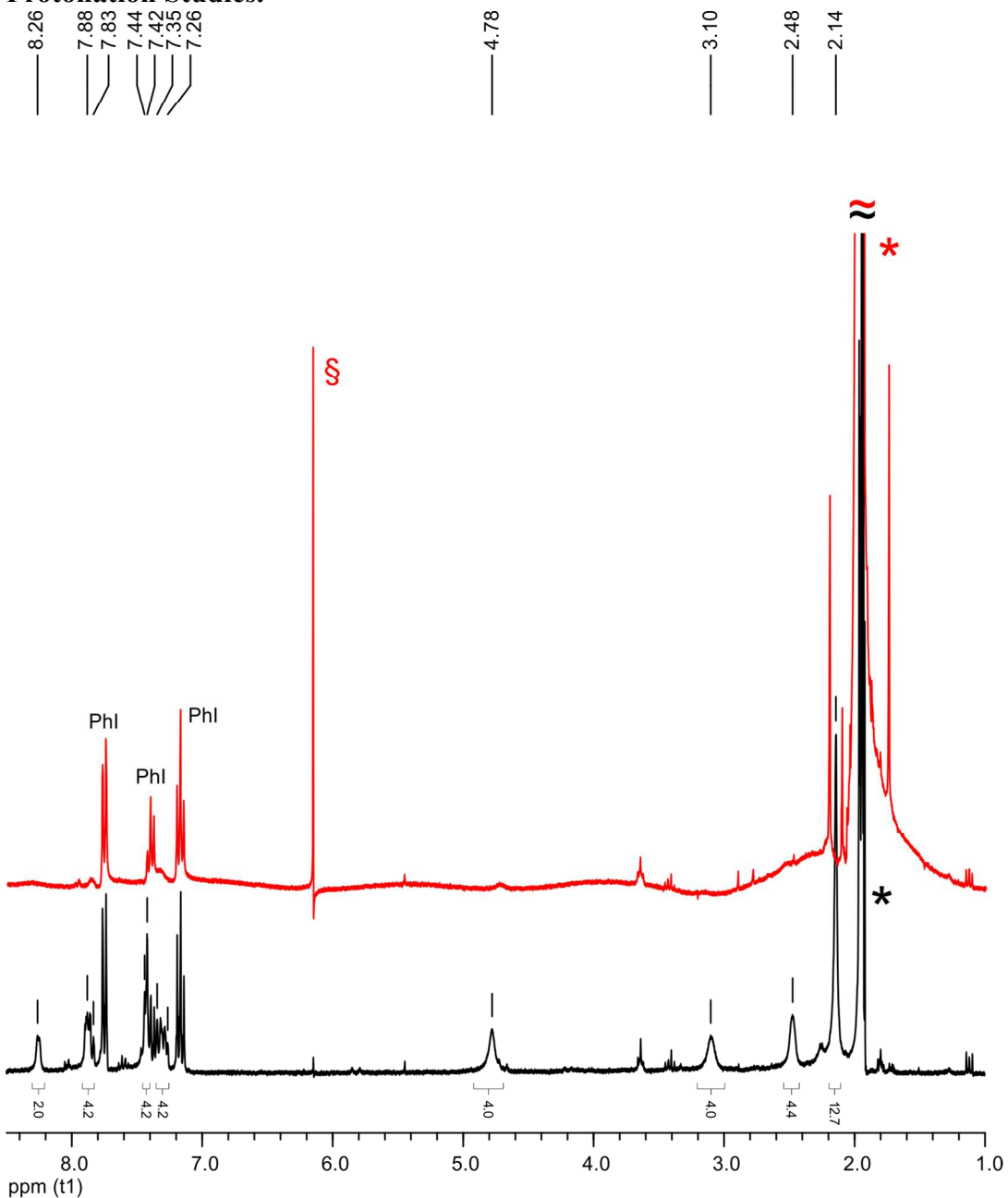
Figure S15. Cutouts of the ^{1}H NMR spectra of solutions of **[FurNeu]**(Cu$_2$(μ-O))(OTf)$_2$, **5**, in acetonitrile-d$_3$ before (black line) and after the addition of 1.2 eq. acetic acid (red line, 0.175 M in acetonitrile). In both cases the asterisk marks the signal of the residual protons in acetonitrile-d$_3$ and the protons of acetonitrile, respectively. § indicates an artifact which is associated with the o1p value of the NMR experiment.
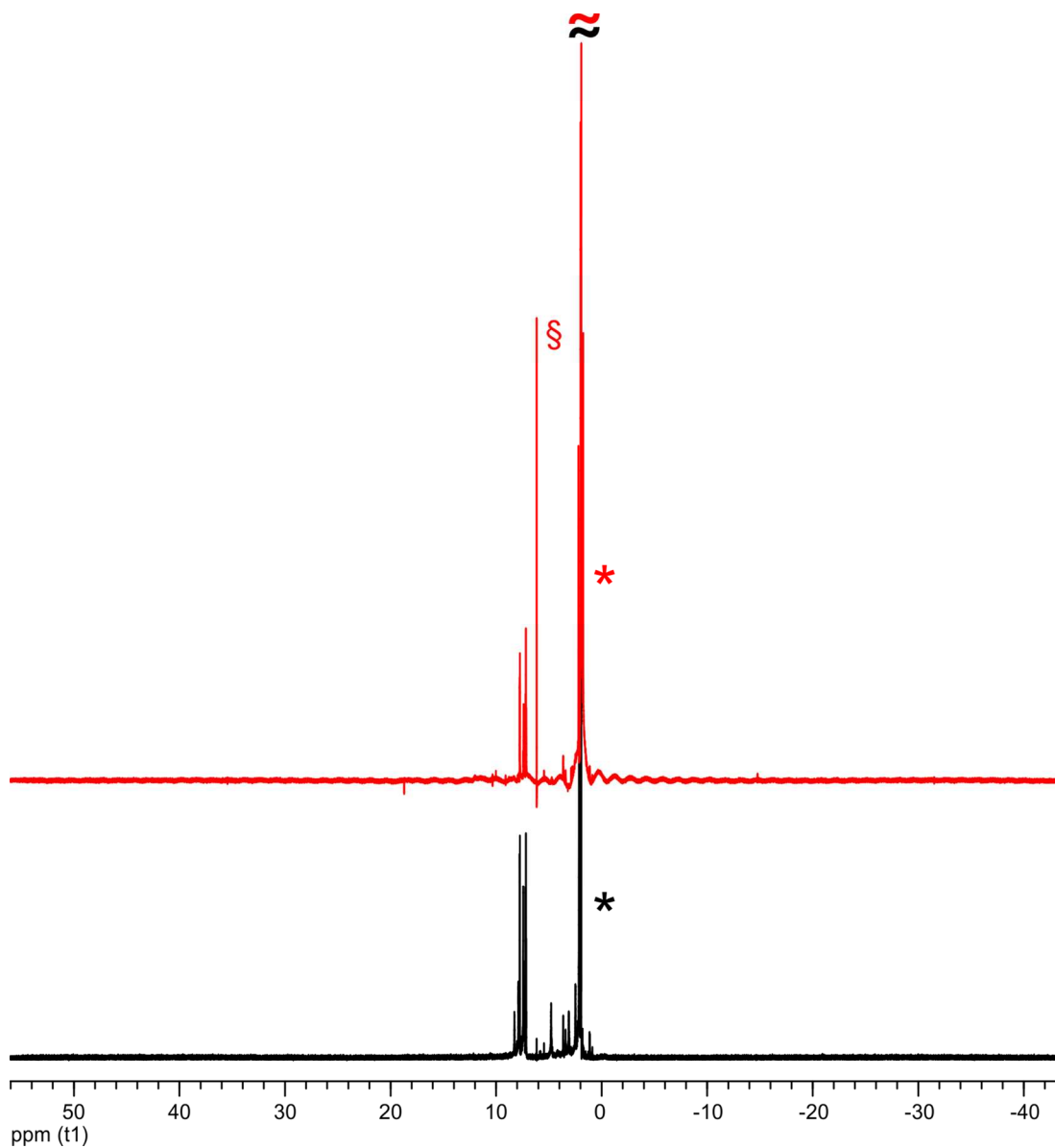
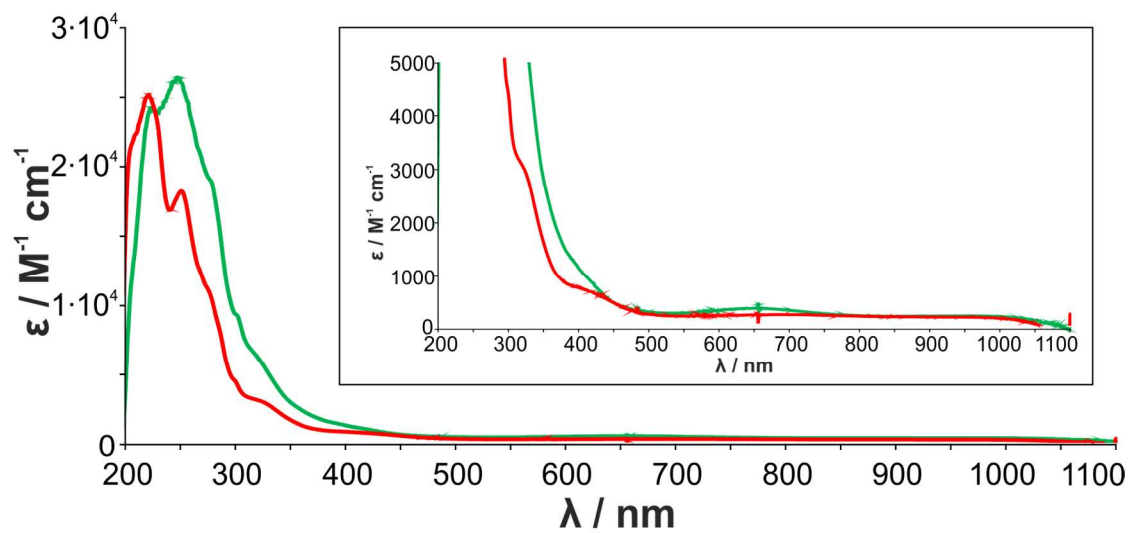**Figure S16.** ^{1}H NMR spectra of solutions of **[FurNeu]**$(Cu_2(\mu\text{-O}))(OTf)_2$, **5**, in acetonitrile-d_3 before (black line) and after the addition of 1.2 eq. acetic acid (red line, 0.175 M in acetonitrile). In both cases the asterisk marks the signal of the residual protons in acetonitrile-d_3 and the protons of acetonitrile, respectively. § indicates an artifact which is associated with the o1p value of the NMR experiment.
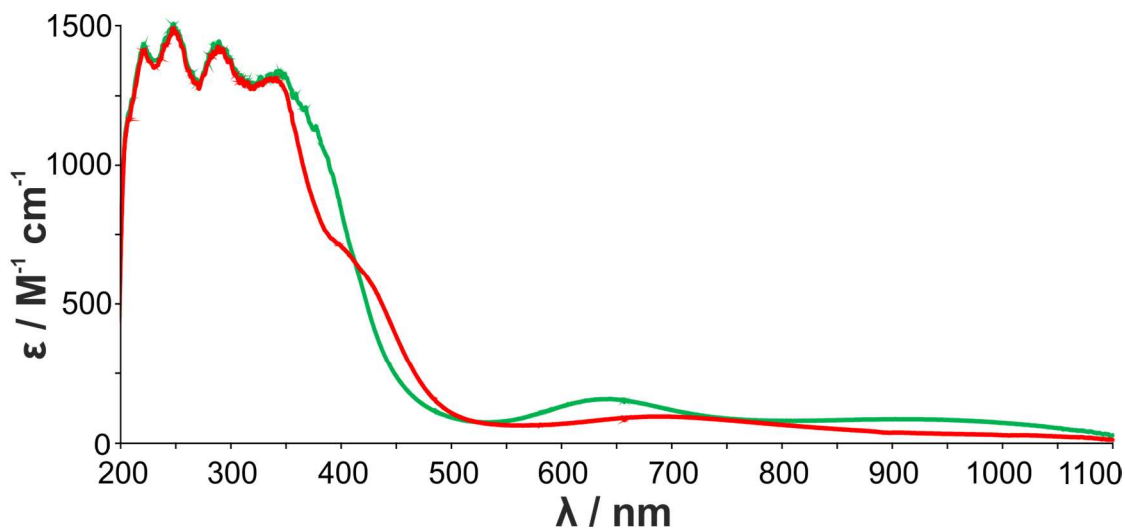
Figure S17. UV/Vis spectra of acetonitrile solutions (2 mM) of **[FurNeu]**$(Cu_2(\mu\text{-O}))(OTf)_2$, **5**, before (green line, generated with PhIO) and after the addition of 1.2 eq. acetic acid (red line, 0.175 M in acetonitrile).
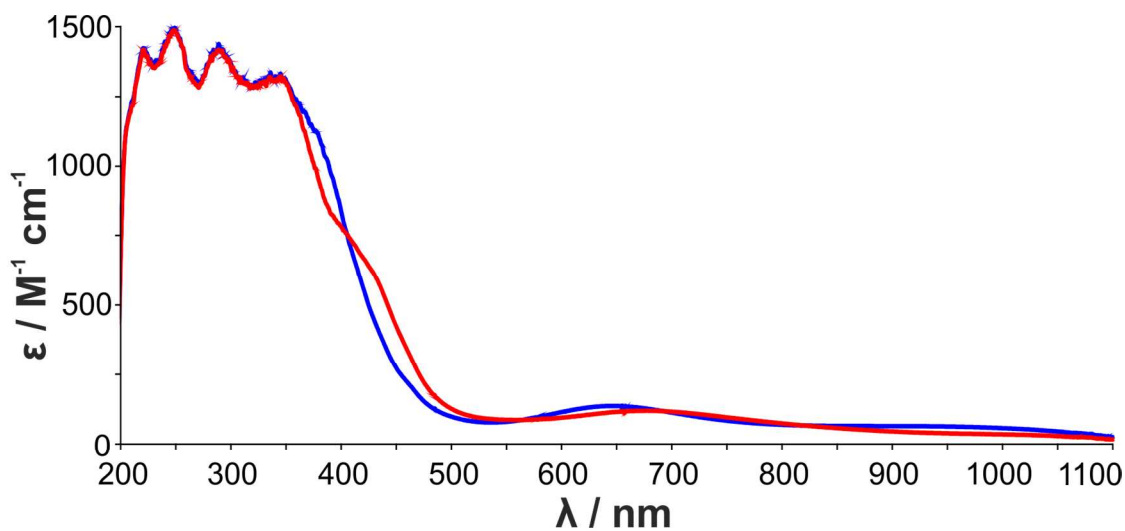

Figure S18. UV/Vis spectra of acetonitrile solutions (2 mM) of **[FurNeu]**$(Cu_2(\mu\text{-O}))(OTf)_2$, **5**, before (blue line, generated with O_2) and after the addition of 1.2 eq. acetic acid (red line, 0.175 M in acetonitrile).
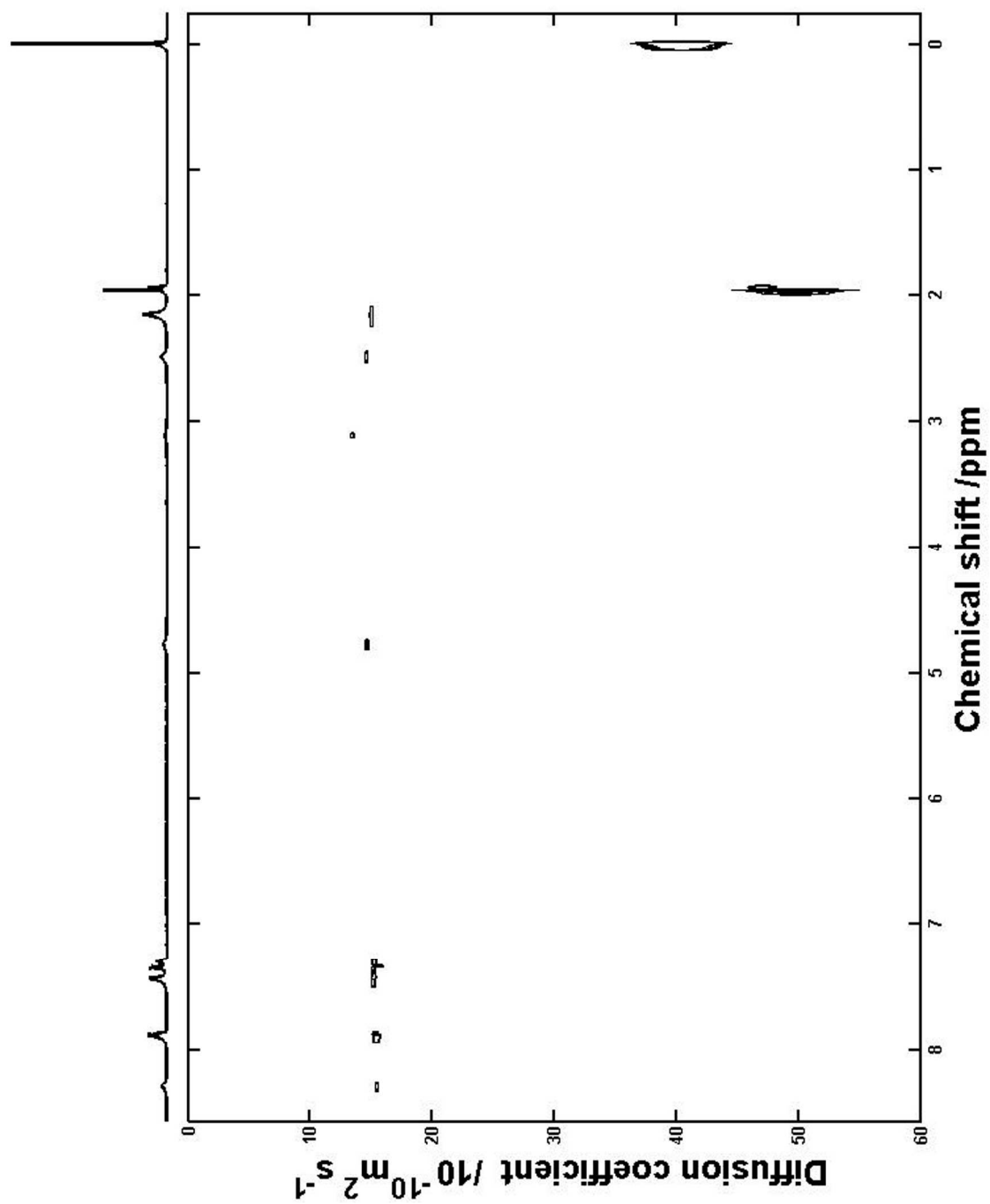
Figure S19. UV/Vis spectra of diluted acetonitrile solutions (0.1 mM) of **[FurNeu]**(Cu$_2$(μ-O))(OTf)$_2$, **5**, before (green line, generated with PhIO) and after the addition of 1.2 eq. acetic acid (red line, 0.175 M in acetonitrile).
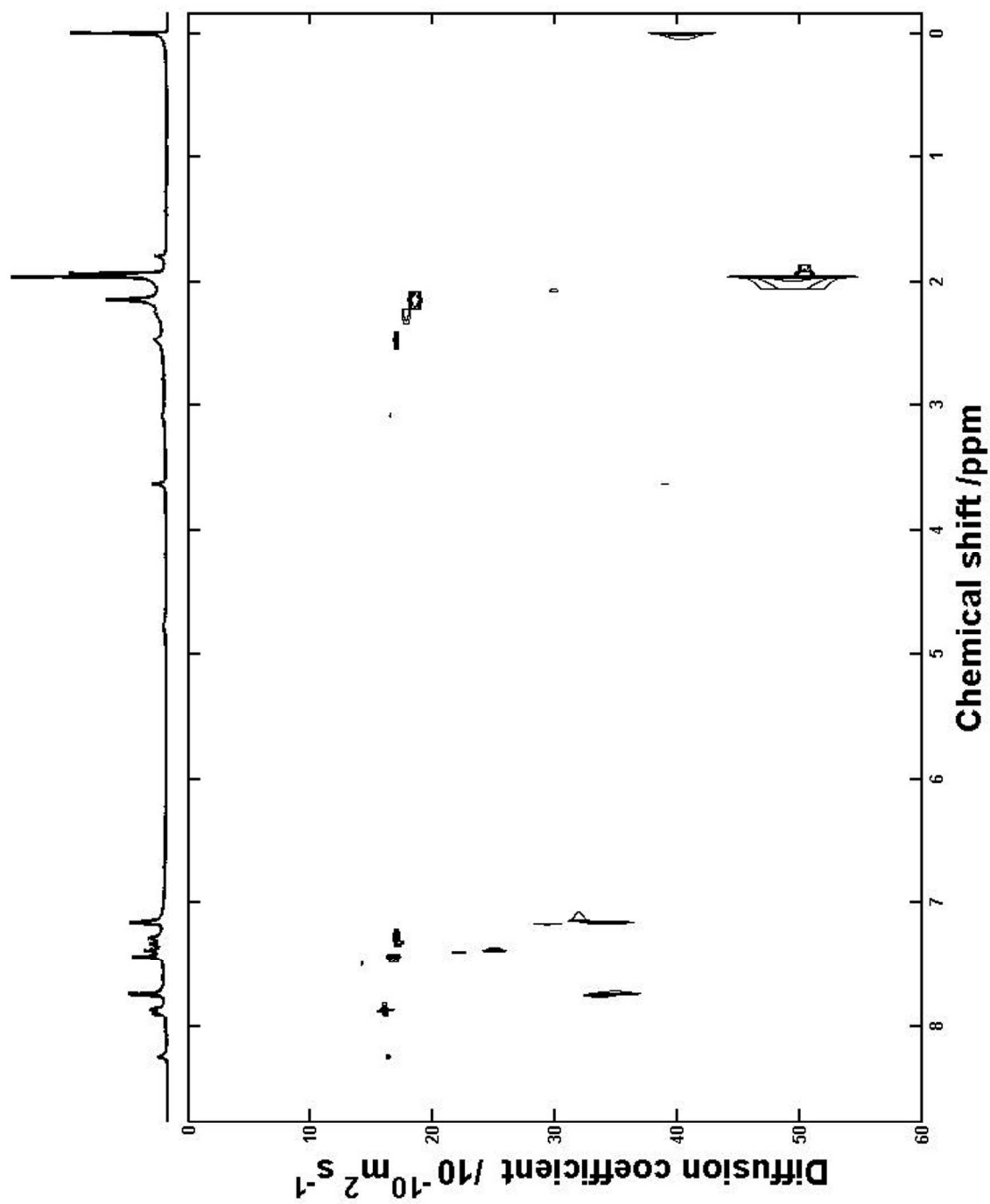
DOSY NMR Spectroscopy.
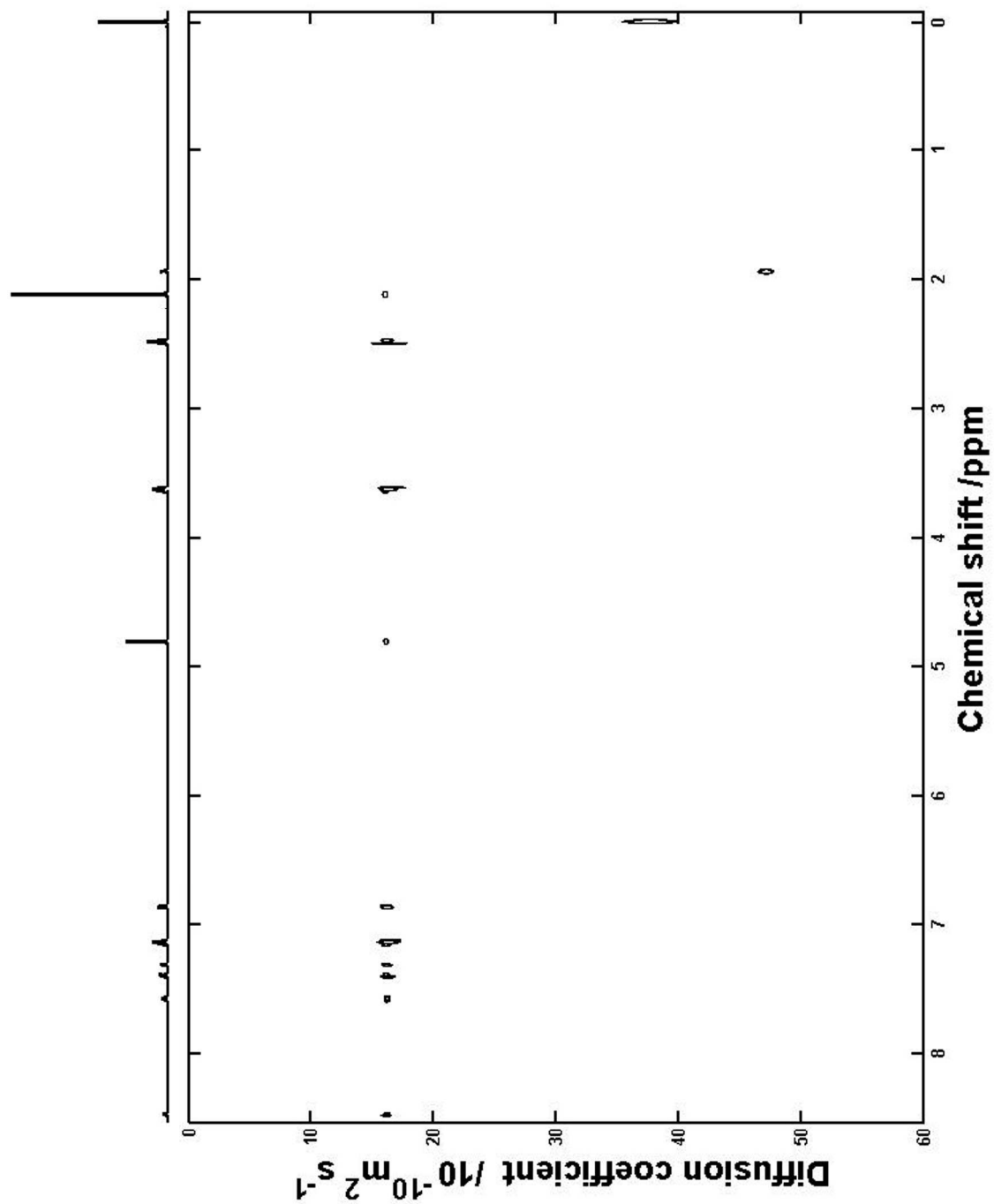
Figure S20. DOSY NMR spectrum of a solution of **FurNeu** in acetonitrile-d$_3$ (including 1 % vol. TMS as a standard) at room temperature.

Figure S21. DOSY NMR spectrum of a solution of **[FurNeu]**(Cu(NCCH$_3$))$_2$(OTf)$_2$, **3**, in acetonitrile-d$_3$ (including 1 % vol. TMS as a standard) at room temperature.

Figure S22. DOSY NMR spectrum of a solution of **[FurNeu]**$(Cu_2(\mu\text{-}O))(OTf)_2$, **5**, in acetonitrile-d_3 (including 1 % vol. TMS as a standard) at room temperature.

- In solution the Stokes-Einstein equation applies: $R_{DOSY} = kT/6\pi\eta D$

- At a constant temperature (T) and viscosity (η) following relation between the radii (R) and diffusion coefficients (D) applies: $R_1/R_2 = D_2/D_1$

- Based on the approximation that the molecules are considered as balls the ratio between the volumes ($V = 4/3*\pi R^3$) is also accessible

-Employment of TMS as a standard allows for the determination of the relative diffusion coefficients: $D_{sample}^{rel} = D_{sample}/D_{TMS}$

FurNeu: D_F = 1.591 D_{TMS} = 3.789 $\mathbf{D_F^{rel} = 0.420 \pm 0.018}$

3: D_3 = 1.485 D_{TMS} = 3.817 $\mathbf{D_3^{rel} = 0.389 \pm 0,018}$

5: D_5 = 1.705 D_{TMS} = 4.210 $\mathbf{D_5^{rel} = 0.405 \pm 0,018}$

FurNeu vs. 3

$D_F^{rel}/D_3^{rel} = 1.08$ $V_3/V_F = 1.26$

Comparing **[FurNeu]**$(Cu(NCCH_3))_2(OTf)_2$, **3**, with the **FurNeu** molecule the volume increases by approx. 26 %.

FurNeu vs. 5

$D_F^{rel}/D_5^{rel} = 1.04$ $V_5/V_F = 1.12$

Comparing **[FurNeu]**$(Cu_2(\mu\text{-}O))(OTf)_2$, **5**, with the **FurNeu** molecule the volume increases by approx. 12 %, indicating that **5** – like **FurNeu** – exists as a **monomer** in solution.

3 vs. 5

$D_3^{rel}/D_5^{rel} = 0.96$ $V_5/V_3 = 0.89$

Comparing **[FurNeu]**$(Cu_2(\mu\text{-}O))(OTf)_2$, **5**, with   **[FurNeu]**$(Cu(NCCH_3))_2(OTf)_2$, **3**, the volume decreases by approx. 11 %, which again points to a **monomeric** character of **5**. The smaller volume of **5** compared to **3** can be ascribed to a lack of coordinated acetonitrile molecules and to the fixation of the N_3-based binding units by the Cu^{II}–O–Cu^{II} entity.

X-ray Absorption Spectroscopy.

XAS measurements were performed on NSLS X3B at Brookhaven National Laboratory in New York, USA, which is equipped with a sagitally focusing Si(111) double-crystal monochromator and a post-monochromator Ni-coated harmonic rejection mirror. Note that while the Ni mirror was in the beam path during data collection, metallic Ni contamination is not significant based on measurement of an experimental blank spectrum. A He Displex cryostat was used for temperature control, with typical sample temperatures of ~20K. Data were collected as fluorescence spectra using a 31 element solid-state Ge detector (Canberra), over an energy range of 8779 – 9853 eV ($k \sim 15$ Å^{-1}). Each scan required approximately 50 minutes. A Cu foil spectrum was collected simultaneously using a photomultiplier tube (PMT) for energy calibration; the first inflection point of the metal foil reference was set to 8979 eV. Scans were collected at several different spots on the sample to test for possible photoreduction effects, as follows:

[FurNeu]$(Cu_2(\mu\text{-O}))(OTf)_2$, **5**: 8 scans at 4 spot, 2 scans per spot.

In addition, XANES data for a Cu metal foil was measured in transmission geometry to provide a genuine Ni^0 standard.

Data averaging was carried out using Athena. All single spectra of the 31 element detector were checked for anomalies and averaged. Reference spectra for individual scans were carefully aligned to ensure that the energy scale was identical for all spectra. Sets of scans at each spot were examined for photoreduction effects. No evidence for photoreduction was observed based upon edge energies and so no scans were excluded from averaged data. Scan sets for individual spots were averaged together and compared with other spots for consistency before being collectively averaged.

EXAFS fitting was carried out using Artemis from the ifeffit package and FEFF6. The FEFF simulation was set on the basis of the DFT structure. Eminent paths from the simulation were selected and combined to obtain the final fit. The fit was evaluated in the k^3 weighted R space. The goodness of the fit was determined on the basis of the R-factor. The significant values of the fitting progress were combined in Table S3.
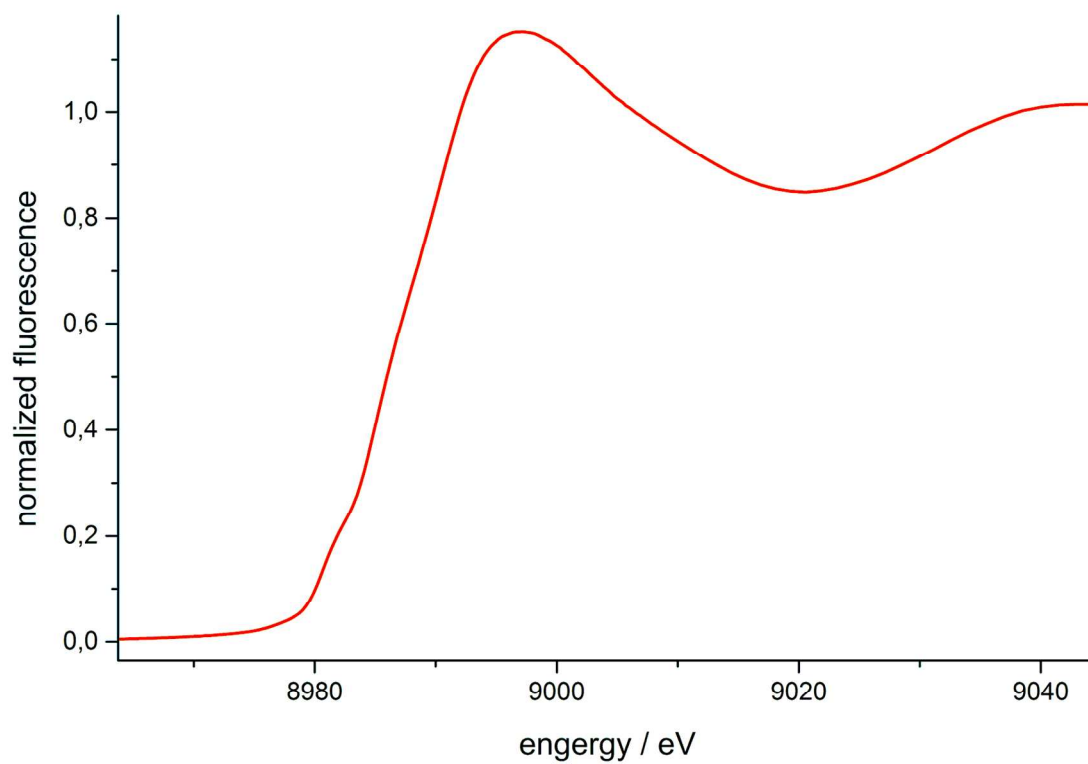
Figure S23. Normalized XANES spectrum of **[FurNeu]**$(Cu_2(\mu\text{-}O))(OTf)_2$, **5**. The Edge Energy is calibrated to a simultaneously measured Cu foil for which the first inflection point was set to 8979 eV.

Table S2. Summary of the EXAFS fitting for the *cis* isomer of **[FurNeu]**$(Cu_2(\mu\text{-}O))(OTf)_2$, **5**.

fit	R-factor	ΔE_0	Cu–O/N			Cu–N/O			Cu–Cu			Cu···C			Cu···N/O			Cu···C			Cu···Cu···O*			Cu···N/O···C*		
			n	r	σ^2	n	r	σ^2	n	r	σ^2	n	r	σ^2	n	r	σ^2	n	r	σ^2	n	r	σ^2	n	r	σ^2
1	0.391	0.49	4	1.93	7.6																					
2	0.339	0.34	1	1.78	13.4	3	1.94	3.4																		
3	0.106	2.75	1	2.11	15.7	3	1.95	3.6	1	2.89	2.9															
4	0.073	-1.36	1	2.36	5.1	3	1.94	3.7	1	2.88	2.6	8	2.73	15.1												
5	0.060	-2.64	1	1.75	10.9	3	1.94	3.0	1	2.88	2.6	8	2.74	15.6	3	4.63	0.4									
6	0.055	-2.45	1	1.75	11.2	3	1.94	3.0	1	2.88	2.6	8	2.74	15.5	3	4.63	0.1	7	4.78	11.0						
7	0.027	-1.03	1	1.79	13.9	3	1.95	3.5	1	2.91	2.6	8	2.81	19.9	3	4.63	0.6	7	4.81	10.1	8	3.26	0.4			
8	**0.022**	**-1.21**	**1**	**1.79**	**13.5**	**3**	**1.95**	**3.5**	**1**	**2.91**	**2.7**	**8**	**2.82**	**19.8**	**3**	**4.63**	**0.9**	**7**	**4.81**	**12.1**	**8**	**3.26**	**0.2**	**16**	**3.77**	**21.9**
9	0.039	0.97				4	1.95	5.9	1	2.93	3.0	8	2.86	19.4	3	4.65	0.9	7	4.86	11.0	8	3.27	-0.2	16	3.80	23.1
10	0.069	1.74	4	1.93	7.8				1	2.93	3.2	8	2.87	16.4	3	4.65	0.9	7	4.88	10.5	8	3.28	-0.5	16	3.81	22.3
11	0.177	4.15	1	2.06	3.1	3	1.94	2.6				8	2.92	4.6	3	4.68	-0.1	7	4.91	6.1				16	3.76	19.3
12	0.185	3.53	1'	1.79	136.1	3'	1.95	3.8				8	2.91	4.6	3	4.67	-0.4	7	4.90	6.2				16	3.77	20.9
13	0.208	3.51	1'	1.79	121.3	3'	1.95	3.8				9	2.91	5.9	3	4.67	-0.6	7	4.90	5.7				16	3.75	18.2
14	0.186	3.49	1'	1.79	132.8	3'	1.95	3.8				8	2.91	4.6	4	4.68	1.0	7	4.91	5.0				16	3.77	21.9
15	0.185	3.53	1'	1.79	134.8	3'	1.95	3.8				8	2.91	4.6	3	4.67	-0.3	8	4.90	8.0				16	3.77	21.2
DFT (*cis*)			1	1.80		3	2.19		1	2.83		8	2.89		3	4.43		7	4.51							

*Multiscattering (2 legs) with a degeneration of 2 for the shown paths and untreated σ² values.

' Fixed radius for this fit.

Fit number 8 (shown bold) is the best fit for the system. r is in units of Å; σ² is in units of 10^{-3} Å; ΔE_0 is in units of eV; R represents the goodness of the fit (GOF) and is defined $R = \sum[(\chi_{dat}(R_i) - \chi_{th}(R_i)^2)/(\chi_{dat}(R_i))^2]$ (value from ifeffit package). Fourier transform ranges: k 2 - 13 Å^{-1}. The fit was optimized in R space with a k-weight of 3. Multiple scattering paths were introduced to improve the fit quality significantly. Fit 9 and 10 demonstrate the importance of the two separate Cu-O/N shells for the quality of the fit.

Table S3. Summary of the binding parameters of **[FurNeu]**$(Cu_2(\mu\text{-O}))(OTf)_2$, **5**, determined by EXAFS spectroscopy.

Shell	n	EXAFS / Å	DFT / Å
Cu–O/N	1	1.79 ± 0.08	1.79
Cu–N/O	3	1.95 ± 0.08	2.20
Cu–Cu	1	2.91 ± 0.08	2.84
Cu···C	8	2.82 ± 0.08	2.89
Cu···N/O	3	4.63 ± 0.08	4.43
Cu···C	7	4.81 ± 0.08	4.51
Cu···Cu···O *	8	3.26 ± 0.08	
Cu···N/O···C *	16	3.77 ± 0.08	

* multiple scattering paths

Reactivity.

PPh$_3$. After the addition of five equivalents of PPh$_3$ a solution of **[FurNeu]**(Cu$_2$(μ-O))(OTf)$_2$, **5**, in acetonitrile changed its color from green to light brown within three hours under anaerobic conditions. Monitoring the reaction with the help of UV/Vis spectroscopy indicated a decrease of the characteristic absorptions bands associated with **5**, and the investigation of the reaction mixture by ^{31}P NMR spectroscopy proved the formation of (O)PPh$_3$ in 8 % yield (with respect to the amount of **3** employed for the generation of **5**). The low efficiency of this oxygen atom transfer may either be rationalized by a steric clash between **5** and the substrate or by a potentially high nucleophilicity of the bridging oxo ligand.[20] Reactivity towards carbon dioxide was not observed and comparable studies employing carbon disulfide as a substrate did not lead to the detection of any dithiocarbonate species.
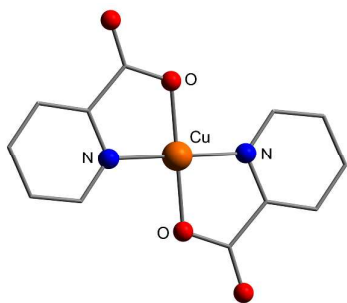
Figure S24. Molecular structure of [Cu(picoloyl)$_2$]. All hydrogen atoms have been omitted for clarity.
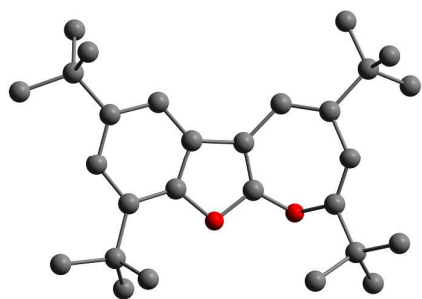
Figure S25. Molecular structure of 2,4,7,9-tetra-*tert*-butyloxepino[2,3-b]benzofuran, TBOBF. All hydrogen atoms have been omitted for clarity.
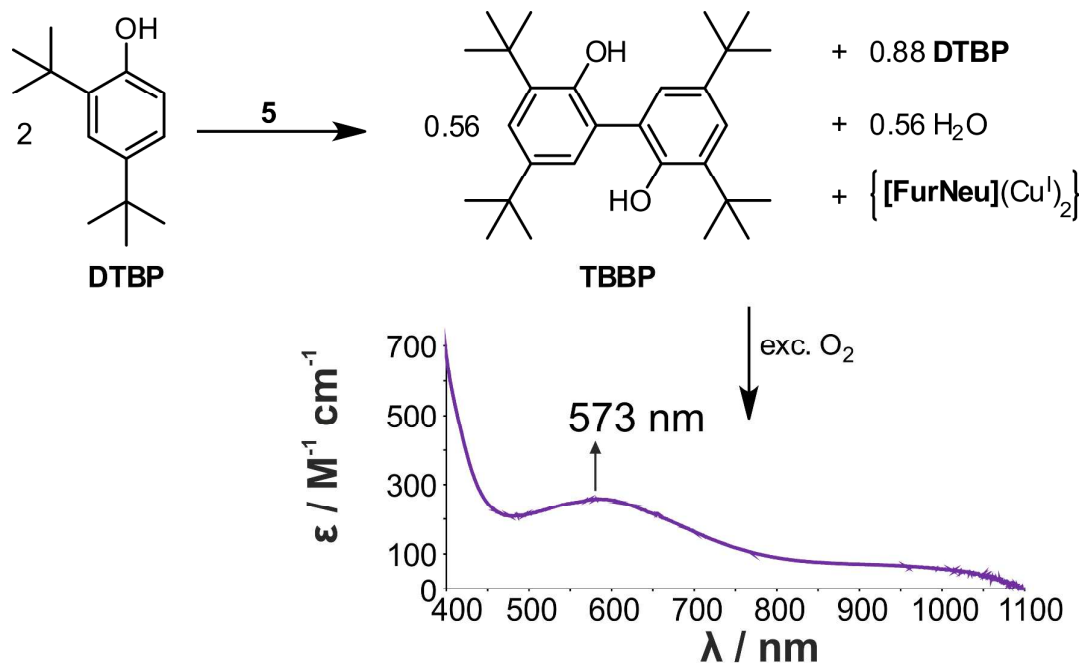
Scheme S4. Summary of the observations made after the investigation of the reaction of **5** with DTBP in acetonitrile at room temperature. Under anaerobic conditions the coupling product TBBP is formed accompanied by the formation of water and a FurNeu based dicopper(I) compound. Subsequent oxygenation of the reaction mixture led to the detection of the UV/Vis spectrum shown at the bottom (2mM with respect to the product originating from the complete conversion of DTBP).
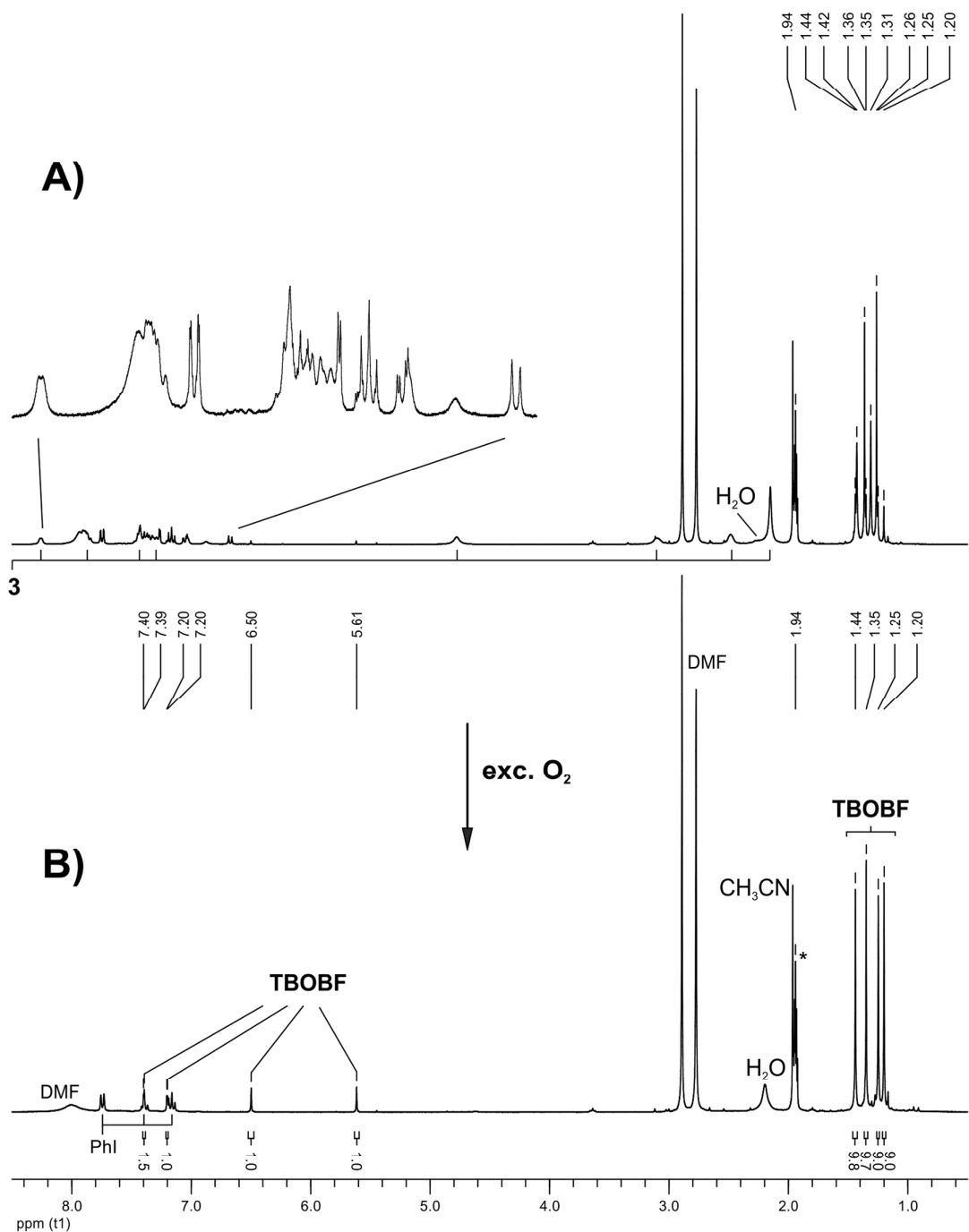
Figure S26. ^{1}H NMR spectra of the reaction solution after **A)** the anaerobic reaction of **[FurNeu]**(Cu$_2$(μ-O))(OTf)$_2$, **5**, with 2 eq. DTBP after 3 hours and **B)** subsequent oxygenation. Spectrum **A)** shows the signal sets deriving from a DTBP/TBBP mixture, the by-product H$_2$O and **[FurNeu]**(Cu(NCCH$_3$))$_2$(OTf)$_2$, **3**, and **B)** shows the spectroscopic features of TBOBF and the by-product H$_2$O. Additionally, **A)** as well as **B)** contain the sets of signals deriving from PhI, CH$_3$CN (by-products formed in the course

of the synthesis of **5**) and dimethylformamide (DMF, internal standard). In both cases acetonitrile-d_3 was employed as the solvent, and the signal of the residual protons is marked with an asterisk.
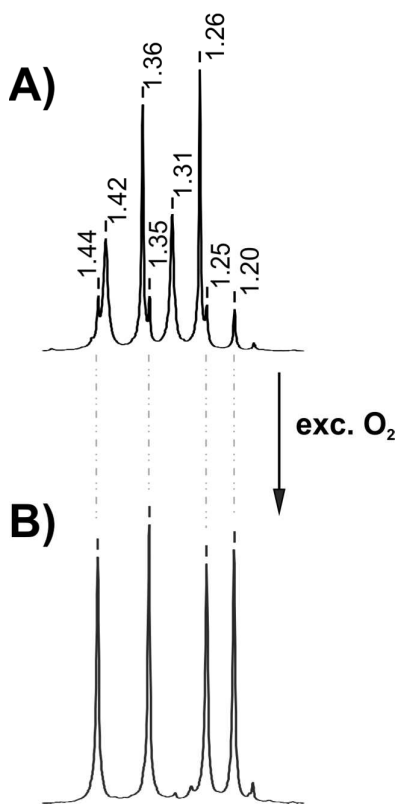
Figure S27. Cutouts from the aliphatic regions in the ^{1}H NMR spectra shown in Figure S13. **A)** 3 hours after the reaction of **[FurNeu]**(Cu$_2$(μ-O))(OTf)$_2$, **5**, with 2 eq. DTBP 0.56 eq. TBBP have formed as determined by integration of the signals corresponding to the *tert*-butyl groups (δ = 1.31, 1.42 ppm). Additionally, the small signals at δ = 1.20, 1.25, 1.35 and 1.44 ppm hint to the formation of traces of TBOBF. **B)** TBOBF has formed as the sole product after oxygenation of the reaction mixture.
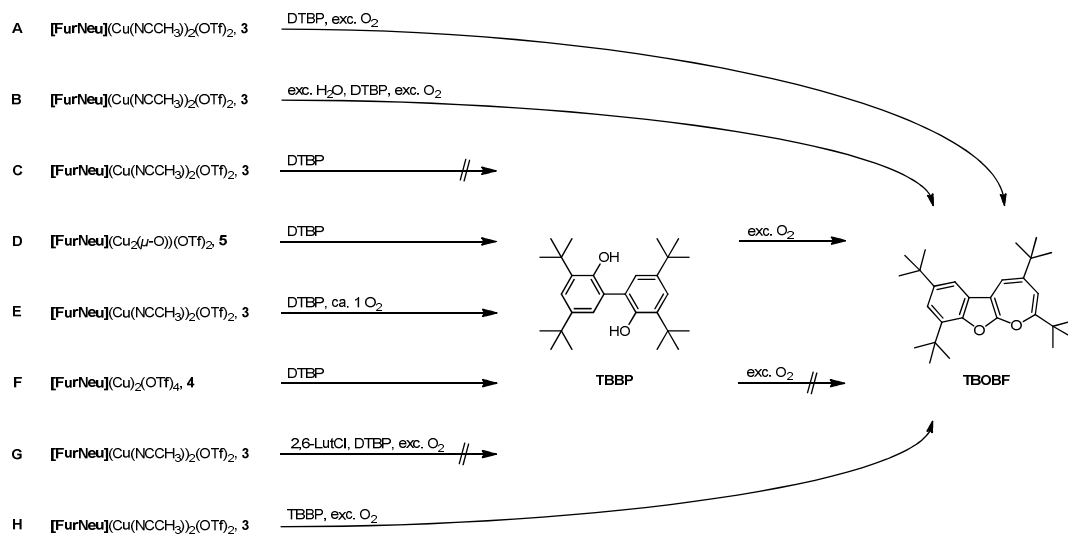
Scheme S5. Summary of the experiments carried out in order to investigate the reactivity of the **FurNeu** based copper complexes **[FurNeu]**$(Cu(NCCH_3))_2(OTf)_2$, **3**, **[FurNeu]**$(Cu_2(\mu\text{-}O))(OTf)_2$, **5**, and **[FurNeu]**$(Cu)_2(OTf)_4$, **4**, towards 2,4-di-*tert*-butylphenol, DTBP, and 3,3',5,5'-tetra-*tert*-butyl 2,2'-biphenol, TBBP, respectively, in presence as well as in absence of dioxygen. TBOBF = 2,4,7,9-tetra-*tert*-butyloxepino[2,3-b]benzofuran.

Table S4. Details of the experiments performed to investigate the reactivity of **[FurNeu]**(Cu(NCCH$_3$))$_2$(OTf)$_2$, **3**, towards 2,4-di-*tert*-butylphenol, DTBP, in presence and absence of O$_2$, respectively. Yields were determined from at least two replicate runs and are given with an accuracy of ±1 %.

m$_{(3)}$ (n$_{(3)}$)	m$_{DTBP}$ (n$_{DTBP}$)	DTBP	O$_2$	Product	yield
10.0 mg (9.71 µmol)	8.0 mg (38.77 µmol)	4 eq.	exc.	TBOBF	100 %
10.0 mg (9.71 µmol)*	8.0 mg (38.77 µmol)	4 eq.	exc.	TBOBF	100 %
5.0 mg (4.85 µmol)	20.0 mg (96.34 µmol)	20 eq.	exc.	TBBP / TBOBF	66 / 15 %
5.0 mg (4.85 µmol)	4.0 mg (19.39 µmol)	4 eq.	≈ 1 eq.	TBBP / TBOBF	36 / 8 %
10.0 mg (9.71 µmol)	8.0 mg (38.77 µmol)	4 eq.	---	---	0 %
5.0 mg (4.85 µmol)**	4.0 mg (19.39 µmol)	4 eq.	exc.	TBOBF	100 %
5.0 mg (4.85 µmol)***	4.0 mg (19.39 µmol)	4 eq.	exc.	---	0 %

* The reaction time amounted to 15 min. ** To the reaction solution an excess of degassed H$_2$O (2 µL, 111 µmol) was added prior to the exposure to O$_2$. *** To the reaction solution 2 eq. of 2,6-lutidinium chloride were added prior the addition of DTBP and the exposure to O$_2$.

Upon employment of stoichiometric and sub-stoichiometric amounts of O$_2$, respectively, the ^{1}H NMR spectrum of the reaction mixture additionally exhibited a set of signals similar to the one caused by **3**:
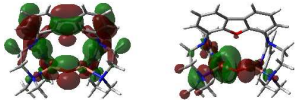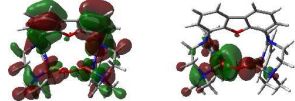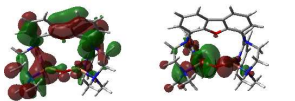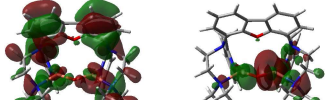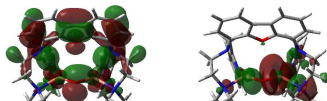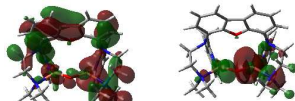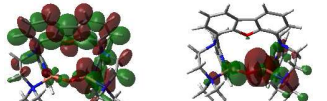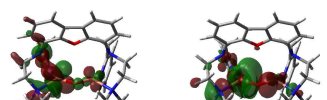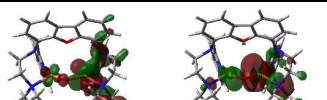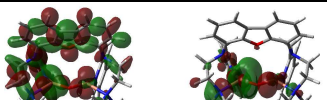
^{1}H NMR (300 MHz, CD$_3$CN): δ [ppm] = 1.96 (s, 6H, C**H**$_3$), 2.16 (s, br, 12H, C**H**$_3$), 2.48 (bt, 4H, C**H**$_2$), 3.11 (br, 4H, C**H**$_2$), 4.78 (br, 4H, C**H**$_2$), 7.27 – 7.38 (m, 4H, C**H**), 7.40 – 7.45 (m, 4H, C**H**), 7.83 – 7.91 (m, 4H, C**H**), 8.27 (d, br, $J(^1$H, ^{1}H) = 4.7 Hz, 2H, C**H**).
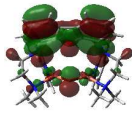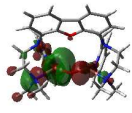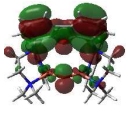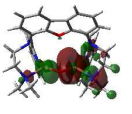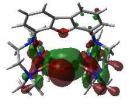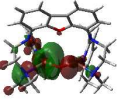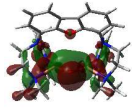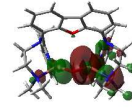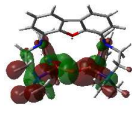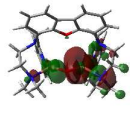
TDDFT Results.

Table S5. Summary of the structural and spectroscopic properties of the *cis* isomer of **[FurNeu]**(Cu$_2$(μ-O))(OTf)$_2$, **5**, and oxygen-activated Cu-ZSM-5[21] determined theoretically and experimentally.

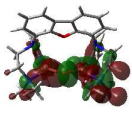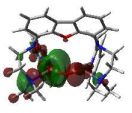|	**5**	**Cu-ZSM-5/O$_2$**
Cu$\cdots$Cu / Å	2.844	3.29
	2.91 (EXAFS)	$\approx$2.9 (EXAFS, not significant)
Cu–O / Å	1.791	1.75/1.76
	1.79 (Cu–O/N, EXAFS)	
Cu–O–Cu / °	105.17	139
ν_s / cm^{-1}	565	456
		456 (exp.)
ν_{as} / cm^{-1}	619	852
		870 (exp.)
Cu–O–Cu bend / cm^{-1}	236	253
		237 (exp.)
λ (Cu^{II} d-d) / nm	648	
	644 (exp.)	752 (exp.)
λ (O$\rightarrow$ Cu^{II} LMCT / nm	<450	
	<450 (exp.)	441 (exp.)

Table S6. Wavelength of TDDFT transitions of the *cis* isomer of **[FurNeu]**(Cu$_2$(μ-O))(OTf)$_2$, **5**, computed at CAM-B3LYP/def2-TZVP level, with specification of the corresponding leading transitions.

Wavelength of transition (nm)	Leading excitations (relative contributions)	Pictorial representation of the leading excitations
843	166α -> 173α (0.08)	
	163α -> 173α (0.07)	
	162α -> 173α (0.07)	
837	163β -> 173β (0.08)	
	166β -> 173β (0.08)	
	162β -> 173β (0.06)	
	155β-> 173β (0.06)	
648	154α -> 173α (0.46)	
	154β -> 173β (0.13)	
	156α -> 173α (0.10)	

416	172α -> 173α (0.14)	
	172β -> 173β (0.13)	
	168α -> 173α (0.08)	
	168β -> 173β (0.07)	
357	167α -> 173α (0.13)	
	167β -> 173β (0.11)	

Table S7. Fractional contribution of basis set functions in the α and β MOs involved in leading TD-DFT excitations at the CAM-B3LYP/def2-TZVP level of the *cis* isomer of **[FurNeu]**$(Cu_2(\mu\text{-}O))(OTf)_2$, **5**. The numbering of atoms on which the p and d basis set functions are centered is assigned based on labels in Figure 8 (see main text).

MO	Fractional contribution of basis set functions
154 (occ.)	α: Cu(2)-d, 0.76 / β: Cu(3)-d, 0.75
155 (occ.)	α: Cu(2)-d, 0.25 / β: Cu(3)-d, 0.28
156 (occ.)	α: Cu(2)-d, 0.32 / β: Cu(3)-d, 0.31
162 (occ.)	α: Cu(2)-d, 0.10; N(6)-p, 0.10 / β: Cu(3)-d, 0.10; N(9)-p, 0.10
163 (occ.)	α: N(7)-p, 0.08 / β: N(4)-p, 0.08
166 (occ.)	α: O(1)-p, 0.18 / β: O(1)-p, 0.18
167 (occ.)	α: N(9)-p, 0.22; O(1)-p, 0.21; Cu(3)-d, 0.12 / β: N(6)-p, 0.22; O(1)-p, 0.21; Cu(2)-d, 0.11
168 (occ.)	α: O(1)-p, 0.50 / β: O(1)-p, 0.51
172 (occ.)	α: O(1)-p, 0.09 / β: O(1)-p, 0.09
173 (virt.)	α: Cu(3)-d, 0.53; O(1)-p, 0.17 / β: Cu(2)-d, 0.53; O(1)-p, 0.17
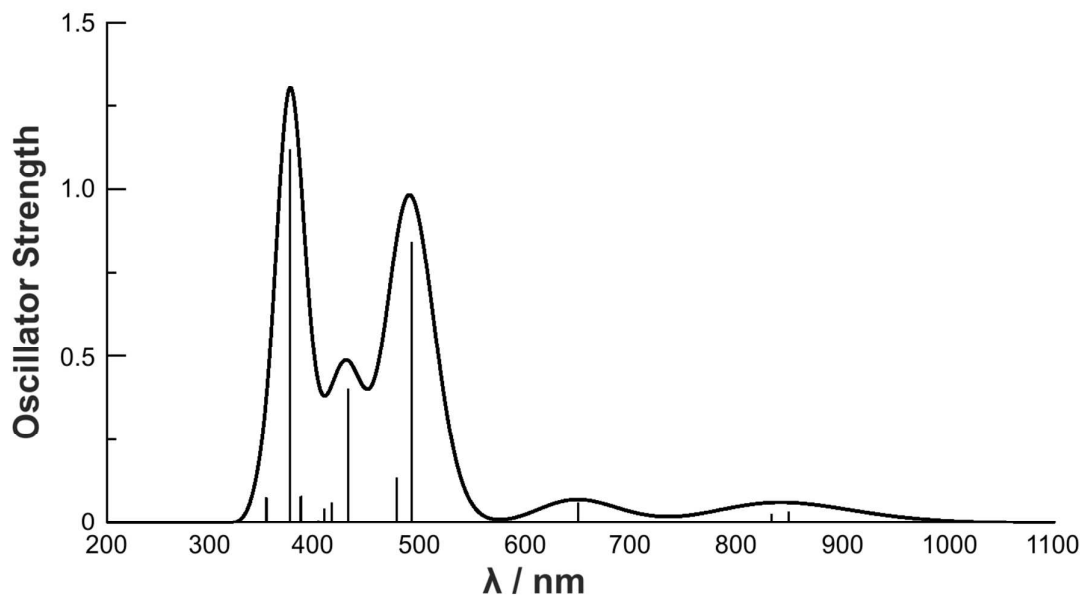
Figure S28. Calculated absorption spectra for the *cis* isomer of **[FurNeu]**$(Cu_2(\mu\text{-O}))(OTf)_2$, **5**, using TDDFT at the CAM-B3LYP/def2-SVP level. The molecular orbitals involved in leading excitations for selected transitions are reported in Table S8. The thicker line represents the Gaussian-broadened spectrum with σ = 900 cm^{-1}.

Table S8. Wavelength of TDDFT transitions of the *cis* isomer of **[FurNeu]**$(Cu_2(\mu\text{-}O))(OTf)_2$, **5**, computed at CAM-B3LYP/def2-SVP level, with specification of the corresponding leading transitions.

| Wavelength of transition (nm)	Leading excitations (relative contributions)
849	164α -> 173α (0.18)
	154α -> 173α (0.16)
	166α -> 173α (0.14)
	169α -> 173α (0.11)
833	164β -> 173β (0.18)
	154β -> 173β (0.15)
	166β -> 173β (0.12)
	169α -> 173β (0.09)
650	156β -> 173β (0.24)
	156α -> 173α (0.20)
	154β -> 173β (0.14)
	154α -> 173α (0.08)
492	169β -> 173β (0.17)
	169α -> 173α (0.10)
	161β -> 173 β (0.07)
	161α -> 173α (0.05)
433	172β -> 173β (0.12)
	172α -> 173α (0.11)
	168β -> 173β (0.05)
	168α -> 173α (0.05)

Table S9. Fractional contribution of basis set functions in the α and β MOs involved in leading TD-DFT excitations at the CAM-B3LYP/def2-SVP level regarding the *cis* isomer of **[FurNeu]**(Cu$_2$(μ-O))(OTf)$_2$, **5**,. The numbering of atoms on which the p and d basis set functions are centered is assigned based on labels in Figure S29 (see below).

MO	Fractional contribution of basis set functions
154 (occ.)	α: Cu(3)-d, 0.58 / β: Cu(2)-d, 0.60
156 (occ.)	α: Cu(3)-d, 0.68 / β: Cu(2)-d, 0.60
161 (occ.)	α: O(1)-p, 0.12 / β: O(1)-p, 0.13
164 (occ.)	α: N(9)-p, 0.10 / β: N(6)-p, 0.09
166 (occ)	α: O(1)-p, 0.17 / β: O(1)-p, 0.17
168 (occ.)	α: O(1)-p, 0.44 / β: O(1)-p, 0.45
169 (occ.)	α: C(10)-p, 0.14; O(1)-p, 0.11; N(4)-p, 0.11/ β: O(1)-p, 0.18; C(11)-p, 0.13; C(12)-p, 0.10.
172 (occ.)	α: O(1)-p, 0.10 / β: O(1)-p, 0.10
173 (virt.)	α: Cu(3)-d, 0.50; O(1)-p, 0.20 / β: Cu(2)-d, 0.60; O(1)-p, 0.20
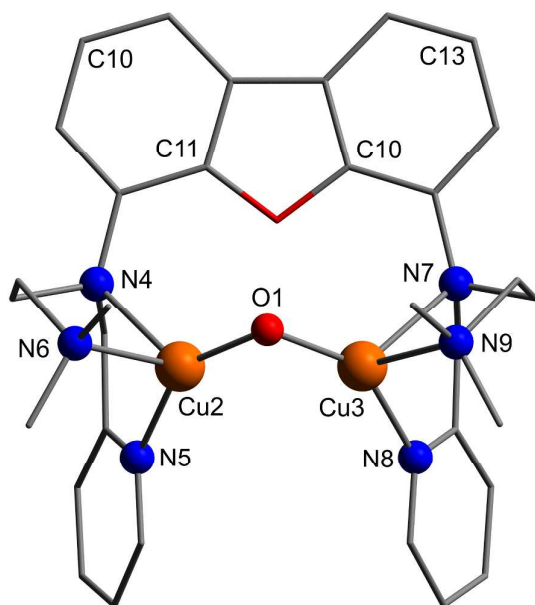
Figure S29. Theoretical structure of the *cis* isomer of the complex cation [[**FurNeu**](Cu$_2$(μ-O))]$^{2+}$ of [**FurNeu**](Cu$_2$(μ-O))(OTf)$_2$, **5**, optimized at B3LYP/def2-SVP level. All hydrogen atoms have been omitted for clarity.
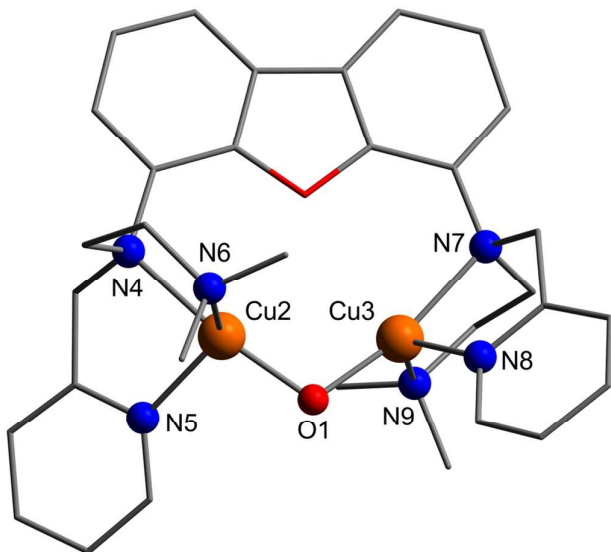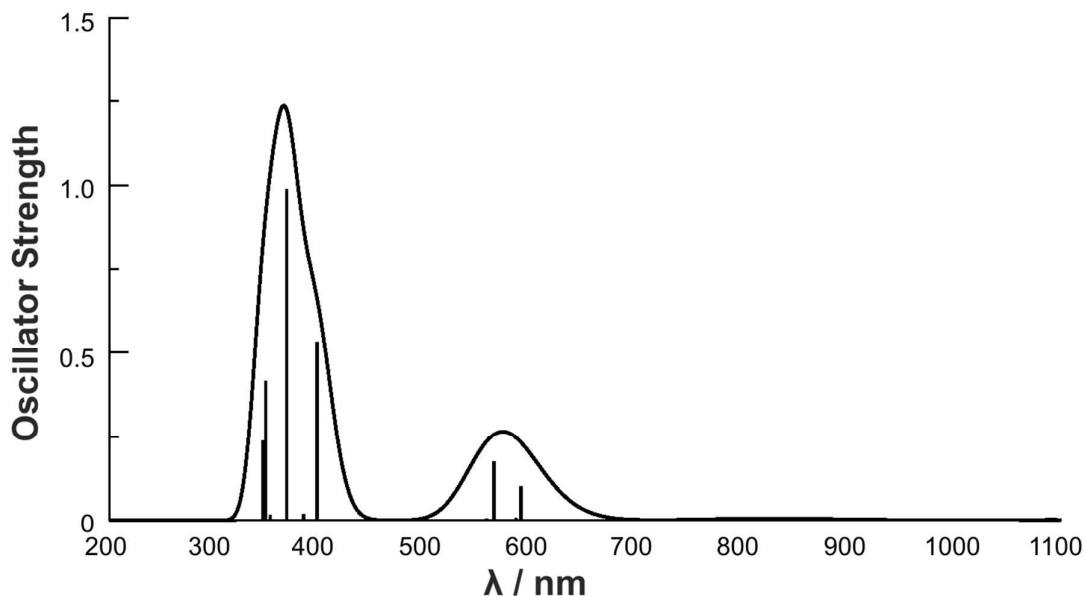
Figure S30. Theoretical structure of the *trans* isomer of the complex cation [[**FurNeu**]$(Cu_2(\mu\text{-}O))]^{2+}$ of [**FurNeu**]$(Cu_2(\mu\text{-}O))(OTf)_2$, **5**, as optimized at B3LYP/def2-TZVP level. All hydrogen atoms have been omitted for clarity. Selected bond lengths [Å] and angles [°]: Cu2···Cu3 2.942, Cu2–O1 1.818, Cu3–O1 1.817, Cu2–N4 2.127, Cu2–N5 2.057, Cu2–N6 2.160, Cu3–N7 2.126, Cu3–N8 2.044, Cu3–N9 2.169, Cu2–O1–Cu3 108.08.

Figure S31. Calculated absorption spectra for the *trans* isomer of **5** using TDDFT at the CAM-B3LYP/def2-SVP level. The molecular orbitals involved in leading excitations for selected transitions are reported in Table S10. The thicker line represents the Gaussian-broadened spectrum with $\sigma = 900$ cm^{-1}.

Table S10. Wavelength of TDDFT transitions for the model of the *trans* isomer of **[FurNeu]**$(Cu_2(\mu\text{-}O))(OTf)_2$, **5**, computed at CAM-B3LYP/def2-SVP level, with specification of the corresponding leading transitions.

Wavelength of transition (nm)	Leading excitations (relative contributions)
608	154β -> 173 β (0.05)
	155β -> 173β (0.29)
	164β -> 173β (0.10)
	166β -> 173β (0.08)
	167β -> 173β (0.21)
601	155α -> 173α (0.30)
	164α -> 173α (0.12)
	166α -> 173α (0.18)

	167α-> 173α (0.08)
584	153α -> 173α (0.26)
	158α -> 173α (0.14)
	153β -> 173β (0.12)
	158β -> 173β (0.27)
	160β -> 173β (0.07)
387	150α -> 173α (0.05)
	172α -> 173α (0.05)
	150β -> 173β (0.06)
	168β -> 173β (0.07)
	172β -> 173β (0.09)
359	168α -> 173α (0.11)
	171α -> 173α (0.10)
	168β -> 173β (0.12)
	171β -> 173β (0.12)

Table S11. Fractional contribution of basis set functions in the α and β MOs involved in leading TD-DFT excitations at the CAM-B3LYP/def2-SVP level regarding the *trans* isomer of **[FurNeu]**$(Cu_2(\mu\text{-O}))(OTf)_2$, **5**,. The numbering of atoms on which the p and d basis set functions are centered is assigned based on labels in Figure S32 (see below).

MO	Fractional contribution of basis set functions
150 (occ.)	α: Cu(13)-d, 0.58; Cu(15)-d, 0.29 / β: Cu(15)-d, 0.36; Cu(13)-d, 0.21
153 (occ.)	α: Cu(15)-d, 0.46 / β: Cu(13)-d, 0.47
154 (occ.)	α: Cu(15)-d, 0.44; Cu(13)-d, 0.19 / β: Cu(13)-d, 0.45; Cu(15)-d, 0.18
155 (occ.)	α: Cu(15)-d, 0.58 / β: Cu(13)-d, 0.57
160 (occ)	α: C(57)-p, 0.10; N(60)-p, 0.10 / β: C(4)-p, 0.10
164 (occ.)	α: N(62)-p, 0.09 / β: C(21)-p, 0.09
166 (occ.)	α: N(62)-p, 0.12 / β: C(58)-p, 0.11; C(59)-p, 0.11; C(56)-p, 0.11; C(55)-p, 0.10.
167 (occ.)	α: C(5)-p, 0.11; C(6)-p, 0.10; C(2)-p, 0.10 / β: N(11)-p, 0.14
168 (occ.)	α: O(14)-p, 0.40 / β: O(14)-p, 0.40; Cu(15)-d, 0.10
171 (occ.)	α: Cu(13)-d, 0.12; O(14)-p, 0.35; N11-p, 0.10 / β: Cu(15)-d, 0.13; N(62)-p, 0.11
172 (occ.)	α: O(14)-p, 0.71 / β: O(14)-p, 0.71
173 (occ.)	α: Cu(15)-d, 0.56; O(14)-p, 0.14 / β: Cu(13)-d, 0.56; O(14)-p, 0.14
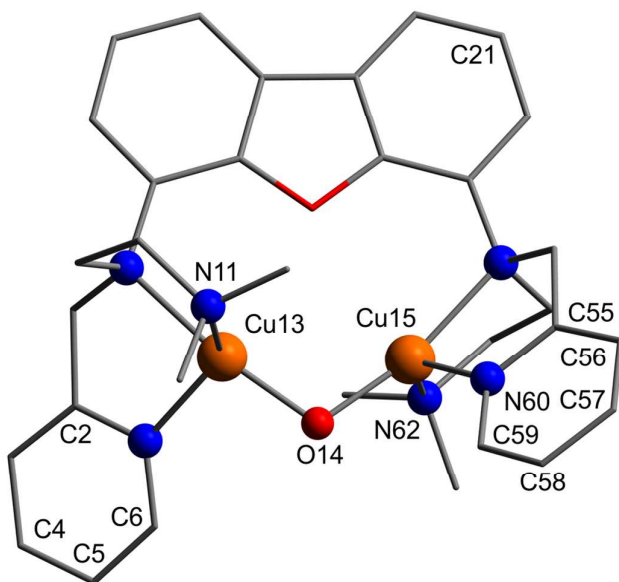
Figure S32. Theoretical structure of the *trans* isomer of the complex cation [[**FurNeu**]($Cu_2(\mu\text{-O})$)]$^{2+}$ of [**FurNeu**]($Cu_2(\mu\text{-O})$)(OTf)$_2$, **5**, optimized at B3LYP/def2-SVP level. All hydrogen atoms have been omitted for clarity.

References.

(1) a) Becke, A. D. *J. Chem. Phys.* **1993,** *98,* 5648. b) Lee, C.; Yang, W.; Parr, R. G. *Phys. Rev. B* **1988,** *37,* 785.

(2) Weigend, F.; Ahlrichs, R. *Phys. Chem. Chem. Phys.* **2005,** *7,* 3297.

(3) Ahlrichs, R.; Baer, M.; Haeser, M.; Horn, H.; Koelmel, C. *Chem. Phys. Lett.* **1989**, *162*, 165.

(4) a) Becke, A. D. *Phys. Rev. A* **1988**, *38*, 3098. b) Perdew, J. P. *Phys. Rev. B* **1986**, *33*, 8822.

(5) a) Salomon, O.; Reiher, M.; Hess, B. A. *J. Chem. Phys.* **2002**, *117*, 4729. b) Reiher, M.; Salomon, O.; Hess, B. A. *Theor. Chem. Acc.* **2001**, *107*, 48.

(6) a) Shiota, Y. ; Juhasz, G.; Yoshizawa, K. *Inorg. Chem.* **2013**, *52*, 7907. b) Shiota, Y.; Yoshizawa, K. *Inorg. Chem.* **2009**, *48*, 838.

(7) Klamt, A. *J. Phys. Chem.* **1995**, 99, 2224.

(8) Yanai, T.; Tew, D. P.; Handy, N. C. *Chem. Phys. Lett.* **2004,** *393,* 51.

(9) Frisch, M. J.; Trucks, G. W.; Schlegel, H. B.; Scuseria, G. E.; Robb, M. A.; Cheeseman, J. R.; Scalmani, G.; Barone, V.; Mennucci, B.; Petersson, G. A.; Nakatsuji, H.; Caricato, M.; Li, X.; Hratchian, H. P.; Izmaylov, A. F.; Bloino, J.; Zheng, G.; Sonnenberg, J. L.; Hada, M.; Ehara, M.; Toyota, K.; Fukuda, R.; Hasegawa, J.; Ishida, M.; Nakajima, T.; Honda, Y.; Kitao, O.; Nakai, H.; Vreven, T.; Montgomery, Jr., J. A.; Peralta, J. E.; Ogliaro, F.; Bearpark, M.; Heyd, J. J.; Brothers, E.; Kudin, K. N.; Staroverov, V. N.; Kobayashi, R.; Normand, J.; Raghavachari, K.; Rendell, A.; Burant, J. C.; Iyengar, S. S.; Tomasi, J.; Cossi, M.; Rega, N.; Millam, N. J.; Klene, M.; Knox, J. E.; Cross, J. B.; Bakken, V.; Adamo, C.; Jaramillo, J.; Gomperts, R.; Stratmann, R. E.; Yazyev, O.; Austin, A. J.; Cammi, R.; Pomelli, C.; Ochterski, J. W.; Martin, R. L.; Morokuma, K.; Zakrzewski, V. G.; Voth, G. A.; Salvador, P.; Dannenberg, J. J.; Dapprich, S.; Daniels, A. D.; Farkas, Ö.; Foresman, J. B.; Ortiz, J. V.; Cioslowski, J.; Fox, D. J. *Gaussian 09*; Gaussian, Inc.: Wallingford CT, 2010., 2011

(10) a) Miertus, S.; Scrocco, E.; Tomasi, J. *Chem. Phys*. **1981,** *55,* 117. b) Barone, V.; Cossi, M.; Tomasi, J. *J. Comput. Chem.* **1998,** *19,* 404.

(11) Cossi, M.; Barone, V. *J. Chem. Phys*. **2001,** *115,* 4708.

(6) Tsang, K. Y.; Diaz, H.; Graciani, N.; Kelly, J. W. *J. Am. Chem. Soc.* **1994,** *116,* 3988.

(7) Bhattacharya, S.; Snehalatha, K.; Kumar, V. P. *J. Org. Chem.* **2003,** *68,* 2741.

(8) Ratilainen, J.; Airola, K.; Fröhlich, R.; Nieger, M.; Rissanen, K. *Polyhedron* **1999,** *18,* 2265.

(9) Dauban, P.; Sanière, L.; Tarrade, A.; Dodd, R. H. *J. Am. Chem. Soc.* **2001,** *123,* 7707.

(10) Schardt, B. C.; Hill, C. L. *Inorg. Chem.* **1983,** *22,* 1563.

(11) Kwong, F. Y.; Klapars, A.; Buchwald, S. L. *Org. Lett.* **2002,** *4,* 581.

(12) a) Zurowska, B.; Mrozinski, J.; Ciunik, Z. *Polyhedron* **2007,** *26,* 1251. b) Kleinstein, A.; Webb, G. *J. Inorg. Nucl. Chem.* **1971,** *33,* 405.

(13) Sheldrick, G. M. *Acta Crystallogr., Sect. A*. **2008,** *64,* 112.

(14) a) Lewis, E. A.; Tolman, W. B. *Chem. Rev.* **2004,** *104,* 1047. b) Hatcher, L. Q.; Karlin, K. D. *J. Biol. Inorg. Chem.* **2004,** *9,* 669.

(15) Woertink, J. S.; Smeets, P. J.; Groothaert, M. H.; Vance, M. A.; Sels, B. F.; Schoonheydt, R. A.; Solomon, E. I. *Proc. Natl. Acad. Sci. USA* **2009,** *106,* 18908.